IEEE Access
Multidisciplinary | Rapid Review | Open Access Journal

Received January 22, 2021, accepted February 2, 2021, date of publication February 5, 2021, date of current version February 17, 2021.

Digital Object Identifier 10.1109/ACCESS.2021.3057378

Feedback Linearized Optimal Control Design for Quadrotor With Multi-Performances

CHUNG-CHENG CHEN[1], AND YEN-TING CHEN[2]
[1]City College of Dongguan University of Technology, Dongguan 523419, China
[2]Department of Electrical Engineering, Graduate School, National Chung Hsing University, Taichung City 402, Taiwan

Corresponding author: Chung-Cheng Chen (ccc49827@ms25.hinet.net)

This work was supported in part by the City College of Dongguan University of Technology under Grant 2017YZDYB01Z.

ABSTRACT Design of tracking controller for quadrotor is an important issue for many engineering fields such as COVID-19 epidemic prevention, intelligent agriculture, military photography and rescue nowadays. This study applies the feedback linearized method and linear quadratic regulator (LQR) method using particle swarm optimization (PSO) to analysis and stabilize the highly nonlinear quadrotor system without applying any nonlinear function approximator that includes neural network approach and fuzzy approach. The article proposes a new method based on the firstly proposed convergence rate formula to achieve the optimal weighting matrices of LQR such that the composite controller can reduce the amplitudes of system control inputs. Determination of the LQR tuning parameters is conventionally achieved via trial and error approach. In addition to being very troublesome, it is difficult to find the globally best tuning matrices with LQR method. This article firstly uses the convergence rate formula of the nonlinear system as the fitness function of LQR approach by using PSO to take the place of the trial and error method. The generalities and implications of proposed approach are globally valid, whereas the Jacobian linearized approach is locally valid due to the Taylor expansion theorem. In addition to these two major achievements, the significant innovation of the proposed method is to possess ''simultaneously'' additional performances including the almost disturbance decoupling, input amplitude reduction, tuning parameter optimization and globally exponential stability performances. Comparative examples show that the convergence rate with our proposed optimal controller using the PSO algorithm is larger than the fuzzy method, and better than the singular perturbation method with high-gain feedback.

INDEX TERMS Almost disturbance decoupling, COVID-19 epidemic prevention, feedback linearized approach, linear quadratic regulator, particle swarm optimization, quadrotor.

I. INTRODUCTION

The air vehicles can be divided into two types including propeller aircraft and jet aircraft according to the engine propulsion method used. Propeller aircraft is a type of fixed-wing aircraft that uses turboprop or reciprocating engines to provide power [1], [2]. Early aircrafts are basically propeller aircrafts. Although jet aircrafts appear later, propeller aircrafts are still widely used. The propeller aircraft can propel forward mainly due to two functions. One is the design of the blade shape, which makes the front and rear air speed difference. According to Bernoulli's law, the resulting speed difference allows the aircraft to gain forward force. The second is the well-known force and reaction force. Pushing the air backward, the aircraft gains forward power. A jet is an aircraft that uses a jet engine as the source of propulsion [3], [4]. It is not same as the traditional propeller aircraft except for the power system used, and the suitable flight environment is also different. Propeller aircrafts need to disturb the surrounding air through the propeller to achieve the purpose of forward propulsion, so it cannot fly in the high altitude where the air density is too thin. On the contrary, due to the different operating principles of the engine, the jet needs to be at an altitude of 10,000 to 15,000 meters and achieve the best propulsion efficiency. Some significant control technologies, such as lift control method [5] and thrust control method [6], have been used to design robust controllers for propeller aircrafts. PID approach [7], model reference adaptive control [8] and backstepping control [8] are applied to address the controller design problem for jet aircrafts. In the past decades,

The associate editor coordinating the review of this manuscript and approving it for publication was Dipankar Deb.

unmanned aerial vehicles have attracted many researches. This research interest is mainly based on the low cost of unmanned aerial vehicle and its large-scale industrial applications in different fields. Among all these drones, quadrotors are considered the most useful due to their flighting modes and simple flighting operations. Quadrotors are widely used in the practical industries including delivery, agriculture, photography, entertainment and rescue [9], [10]. They can fly through complicated structures and check dirty underground tunnel according to their hovering capabilities and maneuverability. Quadrotors have four symmetrical propellers which can produce great thrust in the vertical direction [11]. They have vertical take-off, hovering and landing capabilities like a helicopter. These important functions make them be attractive for many significant industrial applications, such as cooperative operations, academic research and performing tasks in harsh environments.

The researches related to the quadrotors are extensive and many significant approaches, such as model predictive control [12], [13], sliding mode control [14]–[16] and adaptive control [1], [4], [17], [18], have been used to design robust controllers for quadrotors. Reference [19] applied model predictive control for obtaining a precise trajectory with the forcible wind gusts. Model predictive control approach is useful based on its optimal tracking characteristics [20]. Comparisons between this study and [20] are summarized as follows: (i)The existing model predictive control cannot be used to solve the mismatched disturbance case. In contrast, both this study and [20] can completely solve it; (ii)The disturbance effect can be completely cancelled by applying compensation gain in [20]. On the contrary, this study can only almost decouple the disturbance effect; (iii)Deriving the observer gain of [20] needs to solve the complicated differential equation. In contrast, this study only needs to solve algebraic equation. Sliding mode control strategy in [21], [22] shows good robustness to the design of nonlinear system. However, the chattering behaviour is the serious shortcoming which may drive the system to be unstable [23]. Adaptive control approach is usually applied to solve quadrotor system [24]. The shortcoming of adaptive control approach is that the complex updating rule makes it be not practical [25].

For the control of nonlinear system, some performances including the reduction of the disturbance, input command reduction and stability should be simultaneously solved [26]. To address the compromise between these performances, some effective control methods, such as model predictive control [27], deep reinforcement learning [28], multi-objective control [29], backstepping control [30] and preview control [31], have been applied for nonlinear systems. However, in the aforementioned researches, a serious common requirement is that all systems should be approximated to be linear model by using locally Jacobian linearized approach. This requirement may be impractical in the realistic systems. To get over nonlinear behaviours of the realistic systems, function approximators, such as neural network approach [32] and fuzzy logic approach [33], have been applied to minimize the desired performance errors [34]. The neural network approach in [35] is suitable for the control design of nonlinear system and achieves better performances. However, it is a supervised learning approach and needs the system to provide lots of samples. Designing the controller only uses the current state and seriously limits its performance for the neural network method. Moreover, complex coupling structure and computing efforts make the practical realization of nonlinear function approximators be not mature. Building fuzzy control rule actually requires many design experiences and knowledges, and the control performance is closely decided by the chosen rules [36].

It is obvious to see that the robust tracking control issue for quadrotors still is a challenging research due to the difficult stability requirement and disturbances acting on the quadrotor dynamics. Motivated by the aforementioned difficult points, we use feedback linearized approach to design the controller of quadrotor system with the almost disturbance decoupling, input amplitude reduction, tuning parameter optimization, controllable convergence rate and globally exponential stability performances and take the place of traditional LQR trial and error method and Jacobian locally linearized approach. Researches on the feedback linearized approach have made important contributions [37]–[39], and have been widely applied in many engineering applications including the induction motor drive [37], the interior permanent magnet synchronous motors [38], aerial robots [40] and the water pumping [41].

The control strategy partially applied in this article is the linear quadratic regulator (LQR) optimal method. LQR optimal method is an important method to decide the feedback signal for a linear system or linearized system by optimizing the quadratic performance cost index. Appropriate selecting optimal performance cost index, that can achieve the determination of the vector K, results the optimal control system. The optimal K value is decided by the calculation of the famous Riccati equation that needs the input parameters including a semi-positive definite matrix Q and the positive definite matrix R. Comparing the LQR optimal control approach with PID approach yields that LQR has more superior performances [42]. LQR optimal control approach has been applied successfully to many engineering applications. These applications include the control of DC Motor [43], the magnetic levitation system [44], the coupled tank system [45] and the quad-rotor hovering mode [46].

The optimal performance cost index of LQR controller satisfactorily works. However selecting the weighting matrices Q and R is difficult. Some selecting approaches, such as Kalman's pole-assignment approach and genetic algorithm approach, have been investigated in recent researches, but they have strict drawbacks, such as high computing load and low convergent rate of optimal solution [47]. Due to the difficulty of selecting the weighting matrices Q and R, this article proposes a new approach to efficiently obtain them based on particle swarm optimization [48] approach under the guarantee of globally exponential stability. This article has

firstly proposed the convergence rate formula of the nonlinear system as the fitness function of LQR approach by using PSO to take the place of the conventional trial and error method. Moreover, the generality of the proposed approach is global, whereas the Jacobian linearized approach is local [49].

In [50], the strict requirement of almost disturbance decoupling standards for control systems was addressed to depress the disturbances on the output, and then many important related researches have been proposed [51]. However, reference [50] can only solve the ADD problem for nonlinear SISO system subject to the global non-Lipschitz nonlinearity and the nonlinear multiplied disturbance conditions, and then the ADD cannot be well addressed for the control system: $\dot{x}_1(t) = x_2 + w_1(t)$, $\dot{x}_2(t) = u + x_2^3 w_2(t)$, $y_{o1} = x_1 \equiv h_{o1}$, where x_1 and x_2 denote the states, u and y_{o1} are the input and output, respectively, $w_1(t)$ and $w_2(t)$ are the disturbance terms. On the contrary, above system can be well solved by the proposed approach in this article.

The significant novelty of this article is to present optimal controller design for MIMO highly nonlinear quadrotor systems based on feedback linearized and linear quadratic regulator approaches using PSO, and simultaneously achieves the almost disturbance decoupling, input amplitude reduction, tuning parameter optimization, controllable convergence rate, improved suspension and globally exponential stability multiple-performances. Major novelties of this article are summarized as follows:

(i) This study has firstly proposed the convergence rate formula of the nonlinear system as the performance cost index of LQR proc the conventional trial and error approach.

(ii) The quadrotor system is firstly designed by applying the feedback linearized approach and linear quadratic regulator using PSO optimization approach that take the place of using traditional Jacobian linearization method with the almost disturbance decoupling performance.

(iii)An optimal controller is proposed to achieve the global exponential stability without solving the Hamilton-Jacobi equation, that is a complicated partial differential equation with many calculations and needs to be solved for the H-infinity control method.

(iv)In this work, the PSO algorithm is applied to select the optimal weighting matrices Q and R of LQR controller for quadrotor system.

(v) The article gives a method to select the weighting matrices Q and R of linear quadratic regulator such that the composite controller can depress the amplitudes of system inputs.

(vi)The generalities and implications of this approach are globally valid, whereas the locally Jacobian linearized approach is locally valid.

II. OPTIMAL CONTROLLER DESIGN BASED ON PSO AND LQR ALGORITHMS

Consider the linear continuous-time system

$$\dot{\vec{x}} = A\vec{x} + B\vec{u} \tag{1}$$

with the performance cost index

$$J = \frac{1}{2}\vec{x}^T(T_f)S(T_f)\vec{x}(T_f) + \frac{1}{2}\int_{t_0}^{T_f}\left(\vec{x}^T Q\vec{x} + \vec{u}^T R\vec{u}\right)dt \tag{2}$$

where T_f denotes the final time and $S(T_f) \geq 0, Q > 0$, $R > 0$. The main goal of LQR is to find the optimal input for driving the system states from given initial state so that the performance cost index is minimized.

Reference [52] applies the Hamilton-Jacobi-Bellman equation to get the Riccati equation as

$$\dot{S} + Q + SA + A^T S - SBR^{-1}B^T S = 0 \tag{3}$$

and the optimal input is given by

$$\vec{u}^* = -R^{-1}B^T S\vec{x} \tag{4}$$

Selections of the LQR weighting matrices Q and R are generally determined via trial and error operation. In addition to being very troublesome, it is difficult to achieve the best weighting matrices. Up to now, in terms of processing practical systems, there are many optimization techniques [53]–[57] on the existing researches. Some of optimization techniques, such as PSO algorithm [48], [58], [59], genetic algorithm [60], bees algorithm [61], etc. can be applied to adjust optimal LQR weighting matrices. PSO algorithm belongs to be a population-based heuristic optimization technique activated by Eberhart and Kennedy [62]. Compared to other optimization techniques, PSO algorithm has few elements and is easily implemented. In the process of the PSO algorithm, potential particle solutions navigate the problem space by catching the best available solutions. PSO optimization technique basically is handled on the approximation value of the position for the individuals of the swarm to the individual with the best position of the swarm. The initial population is organized by a group of particles. According to the performance cost index, the fitness values of random particles are calculated. The pbest value is the best fitness value and is determined for each particle. The gbest value is the best fitness value ever calculated for all particles in the population, and it is the global best value for the population. According to these obtained pbest and gbest values, the velocities of the particles are determined by (5) and their positions are tuned according to (6). Equation (5) uses the distance between the particle's previous iteration speed, current position, its best experience, and the best experience of the group to update its velocity, and then the particle flies to a new position according to (6).

$$\begin{aligned} v_{ij}^{k+1} &= w \cdot v_{ij}^k + c_1 \cdot r_1 \cdot (pbest_{ij}^k - x_{ij}^k) \\ &\quad + c_2 \cdot r_2 \cdot (gbest_{ij}^k - x_{ij}^k) \end{aligned} \tag{5}$$

$$x_{ij}^{k+1} = x_{ij}^k + v_{ij}^{k+1} \tag{6}$$

where c_1 and c_2 denote learning factors and guide the moving trajectory of the particle based on its own accumulated experience and the accumulated experience of the other particles

in the swarm, respectively. r_1 and r_2 are the random factors located at [0, 1]. w denotes the inertia weighting factor. After the updating procedure, the performance cost index values of all particles in the new population are re-calculated.

The PSO algorithm of acquisition process of learning parameters is shown in Fig. 1 and summarized as follows:

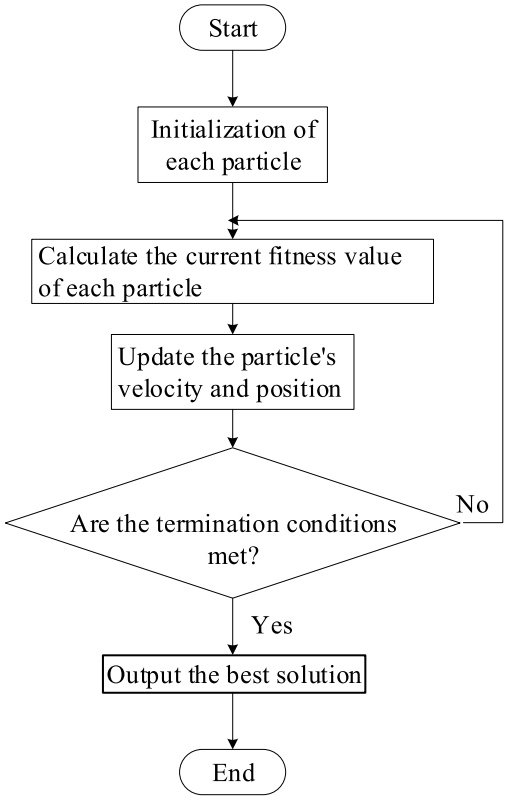

FIGURE 1. Block diagram for the PSO algorithm of acquisition process of learning parameters.

(Step1)Randomly generate m particles, and initialize the position vector x_i^k and velocity v_i^k of each particle. Set initial parameters, including the lower limit L_d and upper limit U_d of the search space, learning factor c_1, c_2, minimum and maximum flight speed $v_{\min}, v_{\max}$, number k of iterations, maximum number $T_{\max}$ of iterations, inertia weight ω and convergence accuracy ς. Choose the current fitness value of each particle to the particle's local optimal value F_i^k and the current initial position x_i^k of each particle to the local best position $pbest_i^k$ of the particle.

(Step 2)Compare the current fitness value of the particle with the current local best value F_i^k of the particle. If it is better than F_i^k, update the individual local best value F_i^k and update the local best position $pbest_i^k$ of the particle to the current location.

(Step 3)Find the best fitness extreme value of the current population from all particles by $\min(F_1^*, F_2^*, \cdots F_m^*)$. If this extreme value is better than the current global best extreme value F_g^k, update the global best value F_g^k and update $gbest_i^k$ to the position of the particle represented by this extreme value.

(Step 4)Use (5) and (6) to update the particle's velocity and position, respectively, and increase k to be k+1. If the moving distance v_{id}^{k+1} of the new velocity v_i^{k+1} in a certain dimension of the spatial coordinates is greater than $v_{\max}$, then update it to $v_{\max}$. If v_{id}^{k+1} is less than $v_{\min}$, then update it to $v_{\min}$. If the moving distance x_{id}^{k+1} of the new position x_i^{k+1} in a certain dimension of the spatial coordinates is greater than U_d, then update it to U_d. If x_{id}^{k+1} is less than L_d, then update it to L_d.

(Step 5)If the current iteration number k reaches the preset maximum number $T_{\max}$ or the final result is less than the predetermined convergence accuracy ς, stop the iteration and output the best solution.

Here is a more detailed explanation as follows. The random factors r_1 and r_2 are used to maintain the diversity of group movement directions. c_1 can bring the particle closer to its own historical best point, so it is also called the cognitive learning factor. c_2 can make the particle approach the best point in the history of the group, so it is also called the social learning factor. Generally speaking, c_1 and c_2 are set to two. When the inertial weight w is large ($w > 1.2$), PSO algorithm tends to explore new areas on a large scale. At this time, PSO algorithm is a global search method. When the inertial weight w is small ($w < 0.8$), PSO algorithm tends to find the best value in a local area, and PSO algorithm is a local search method at this time. Therefore, if the inertia weight is linearly decreased in the iterative calculation process, the PSO algorithm has a good global search ability at the beginning, and can quickly locate the area close to the best solution in the entire domain. In the later stage, it has a good local search ability to accurately obtain the best global solution. The general literature suggests that decreasing from 0.9 to 0.4 is the best choice. The linearly decreased formula is given by

$$w = w_{start} - [(w_{start} - w_{end})/T_{\max}] \times n \tag{7}$$

where n is the current number of iterations, $T_{\max}$ denotes the maximum number of iterations, w_{start} is the initial inertia weight and w_{end} is inertia weight of termination.

III. FEEDBACK LINEARIZED AND LINEAR QUADRATIC REGULATOR USING PSO COMPOSITE CONTROLLER DESIGN

In this article, we consider the general nonlinear system with disturbances to construct a composite feedback linearized and LQR controller using PSO with almost disturbance decoupling, input amplitude reduction, tuning parameter optimization, controllable convergence rate, improved suspension and globally exponential stability multi-performances:

$$\begin{aligned}&\left[\dot{x}_1 \cdots \dot{x}_n\right]^T \\ &\quad = \left[f_1(\vec{X}) \cdots f_n(\vec{X})\right]^T \\ &\qquad + \left[\vec{g}_1(\vec{X}) \cdots \vec{g}_m(\vec{X})\right]\left[u_1(\vec{X}) \cdots u_m(\vec{X})\right]^T \\ &\qquad + \sum_{j=1}^{p} \vec{q}_j^{\,*}\left(\theta_j\right)\end{aligned} \tag{8}$$

$$\left[y_{o1}(\vec{X}) \cdots y_{om}(\vec{X}) \right]^T = \left[h_{o1}(\vec{X}) \cdots h_{om}(\vec{X}) \right]^T \quad (9)$$

i.e.,

$$\dot{\vec{X}}(t) = \vec{f}(\vec{X}(t)) + \underset{\sim}{\rightarrow} g(\vec{X}(t))\vec{u} + \sum_{j=1}^{p} \vec{q}_j^* \left(\theta_j\right) \quad (10)$$

$$\vec{y}_o(t) = \vec{h}_o(\vec{X}(t)) \quad (11)$$

where $\vec{X}(t) \equiv [x_1(t)\, x_2(t) \cdots x_n(t)]^T$ is the system state vector, $\vec{u} \equiv [u_1 u_2 \cdots u_m]^T$ denotes the control vector, $\vec{y}_o \equiv [y_{o1} y_{o2} \cdots y_{om}]^T$ denotes the desired output vector, $\vec{q}_j^*$ denotes the adjoint constant vector, $\vec{\theta} \equiv \left[\theta_1(t)\ \theta_2(t) \cdots \theta_p(t)\right]^T$ is the disturbances vector, $\vec{f} \equiv [f_1 f_2 \cdots f_n]^T$, $\underset{\sim}{\rightarrow} g \equiv \left[\vec{g}_1 \vec{g}_2 \cdots \vec{g}_m\right]$ and $\vec{h}_o \equiv [h_{o1} h_{o2} \cdots h_{om}]^T$ are infinitely continuous vector fields. Define the nominal system to be

$$\dot{\vec{X}}(t) = \vec{f}(\vec{X}(t)) + \underset{\sim}{g}(\vec{X}(t))\vec{u} \quad (12)$$

$$\vec{y}_o(t) = \vec{h}_o(\vec{X}(t)) \quad (13)$$

and has the vector relative degree $\{r_{o1}, r_{o2}, \cdots, r_{om}\}$ [63], [64]:

<i> the following equation holds:

$$L_{\vec{g}_j} L_{\vec{f}}^k h_{oi}(\vec{X}) = 0 \quad (14)$$

for all $1 \le i, j \le m, k < r_{oi} - 1$, where the operator L is the Lie derivative.

<ii> The $m \times m$ matrix

$$A \equiv \begin{bmatrix} L_{g_1} L_f^{r_{o1}-1} h_{o1}(\vec{X}) & \cdots & L_{g_m} L_f^{r_{o1}-1} h_{o1}(\vec{X}) \\ \vdots & & \vdots \\ L_{g_1} L_f^{r_{om}-1} h_{om}(\vec{X}) & \cdots & L_{g_m} L_f^{r_{om}-1} h_{om}(\vec{X}) \end{bmatrix} \quad (15)$$

is a nonsingular matrix. The desired tracking signals y_{od}^i, $1 \le i \le m$ and its first r_{oi} derivatives are bounded as:

$$\left\| \left[y_{od}^i,\ y_{od}^{i\ (1)}, \cdots, y_{od}^{i\ (r_{oi})} \right] \right\| \le B_{od}^i,\ 1 \le i \le m$$

where B_{od}^i are positive constants and the distribution

$$G \equiv span\{\vec{g}_1, \vec{g}_2, \cdots, \vec{g}_m\} \quad (16)$$

has involutive property. Therefore, reference [63] had exploited the fact that the function

$$\phi : \Re^n \to \Re^n \quad (17)$$

described as

$$\vec{\xi}_i \equiv \left[\xi_1^i \cdots \xi_{r_{oi}}^i \right]^T \equiv \left[\phi_1^i \cdots \phi_{r_{oi}}^i \right]^T \equiv \left[L_{\vec{f}}^0 h_{oi}(\vec{X}) \cdots L_{\vec{f}}^{r_{oi}-1} h_{oi}(\vec{X}) \right]^T \quad (18)$$

$$\phi_k(\vec{X}(t)) \equiv \eta_k(t), k = r_o + 1, r_o + 2, \cdots, n \quad (19)$$

and satisfying

$$L_{g_j} \phi_k(\vec{X}(t)) = 0, k = r_o + 1, r_o + 2, \cdots, n, 1 \le j \le m \quad (20)$$

is a bijective and infinitely continuous function.

The above bijective and infinitely continuous function will convert the full nonlinear quadrotor system into a controllable system including the partially nonlinear subsystem (19) and the partially linear subsystem (18). Parameters $\xi_{r_{om}}^m$ and η_k denote the state variables of the partially linear subsystem and partially nonlinear subsystem, respectively. In order to achieve the tracking performance, define

$$e_j^i \equiv \xi_j^i - y_{od}^{i(j-1)} \quad (21)$$

$$e^i \equiv \left[e_1^i\ e_2^i \cdots e_{r_{oi}}^i \right]^T \in \Re^{r_i} \quad (22)$$

$$\overline{e_j^i} \equiv \varepsilon^{j-1} e_j^i,\ i = 1, 2, \cdots, m, j = 1, 2, \cdots, r_{oi} \quad (23)$$

$$\overline{e^i} \equiv \left[\overline{e_1^i}\ \overline{e_2^i} \cdots \overline{e_{r_{oi}}^i}(t) \right]^T \in \Re^{r_{oi}} \quad (24)$$

$$\overline{e} \equiv \left[\overline{e^1}\ \overline{e^2}\ \cdots\ \overline{e^m} \right]^T \in \Re^{r_o} \quad (25)$$

$$\vec{\xi} \equiv \left[\xi_1\ \xi_2\ \cdots\ \xi_{r_o} \right]^T \quad (26)$$

$$\vec{\eta} \equiv \left[\eta_{r_o+1}\ \eta_{r_o+2} \cdots \eta_n \right]^T \quad (27)$$

$$\vec{\rho}(\vec{\xi}, \vec{\eta}) \equiv \left[L_f \phi_{r_o+1}\ L_f \phi_{r_o+2} \cdots L_f \phi_n \right]^T \equiv \left[\rho_{r_o+1}\ \rho_{r_o+2}\ \cdots\ \rho_n \right]^T \quad (28)$$

$$A_c^i \equiv \begin{bmatrix} 0 & 1 & 0 & \cdots & 0 \\ 0 & 0 & 1 & \cdots & 0 \\ & \vdots & & & \vdots \\ 0 & 0 & 0 & \cdots & 1 \\ -\alpha_1^i & -\alpha_2^i & -\alpha_3^i & \cdots & -\alpha_{r_{oi}}^i \end{bmatrix}_{r_{oi} \times r_{oi}} \quad (29)$$

$$\vec{B}^i \equiv \left[0\ 0 \cdots 0\ 1 \right]_{r_{oi} \times 1}^T, 1 \le i \le m \quad (30)$$

where $\alpha_1^i, \alpha_2^i, \cdots, \alpha_{r_{oi}}^i$ are adjustable constants such that A_c^i are Hurwitz matrices and $P^i > 0$ are the solutions of the Lyapunov equation described as.

$$(A_c^i)^T P^i + P^i A_c^i = -I \quad (31)$$

$$\nabla_{\max}(P^i) \equiv \text{the maximum eigenvalue of } P^i \quad (32)$$

$$\nabla_{\min}(P^i) \equiv \text{the minimum eigenvalue of } P^i \quad (33)$$

$$\nabla_{\max}^* \equiv \max \left\{ \nabla_{\max}(P^1),\ \nabla_{\max}(P^2), \cdots, \nabla_{\max}(P^m) \right\} \quad (34)$$

$$\nabla_{\min}^* \equiv \min \left\{ \nabla_{\min}(P^1),\ \nabla_{\min}(P^2), \cdots, \nabla_{\min}(P^m) \right\} \quad (35)$$

Assumption 1: Exists a positive number M_{non} such that the following condition holds, for $t \ge 0$, $\vec{\eta} \in \Re^{n-r_o}$ and $\vec{\xi} \in \Re^{r_o}$:

$$\left\| \vec{\rho}_{non}(t, \vec{\eta}, \bar{e}) - \vec{\rho}_{non}(t, \vec{\eta}, 0) \right\| \le M_{non}\left(\|\bar{e}\|\right) \quad (36)$$

where $\vec{\rho}_{non}(t, \vec{\eta}, \bar{e}) \equiv \vec{\rho}(\vec{\xi}, \vec{\eta})$.

To analysis precisely the controller design of quadrotor system, let

$$u_{dij} \equiv L_{\vec{g}_j} L_{\vec{f}}^{r_{io}-1} h_{oi}(\vec{X}) \tag{37}$$

$$u_{ci} \equiv L_f^{r_{oi}} h_{oi}(\vec{X}) \tag{38}$$

$$\overline{\overline{e^i}} \equiv \alpha_1^i \overline{e_1^i} + \alpha_2^i \overline{e_2^i} + \cdots + \alpha_{r_{oi}}^i \overline{e_{r_{oi}}^i} \tag{39}$$

and give two definitions as follow [65]:

Definition 1: Consider a nonlinear system $\dot{\vec{x}} = \vec{f}(t, \vec{x}, \vec{u})$ with an input $\vec{u}$, where $\vec{x}$ is state vector, $a_{22} \equiv -0.0578 - 0.0578\left(-x_1^2 + x_2^2 - x_3^2\right)$, is infinitely continuous and $\vec{x}$, $\vec{u}$ are Lipschitz. This system is input-to-state stable if exists a K-class function β and KL-class function γ such that

$$\left\|\vec{x}(t)\right\| \le \gamma\left(\left\|\vec{x}(t_0)\right\|, t - t_0\right) + \beta\left(\sup_{t_0 \le \tau \le t}\left\|\vec{u}(\tau)\right\|\right) \tag{40}$$

Definition 2: The almost disturbance decoupling performance is achievable with noise input $\vec{\theta}_{noise}$ for a control system, if the following conditions hold:

<i> The control system is input-to-state stable with noise input $\vec{\theta}_{noise}$

<ii> The desired output tracking errors satisfy the following conditions:

$$\left|y_{oi}(t) - y_{od}^i(t)\right| \le \beta_{11}\left(\left\|\vec{x}(t_0)\right\|, t - t_0\right) + \frac{1}{\sqrt{\beta_{22}}}\beta_{33}\left(\sup_{t_0 \le \tau \le t}\left\|\vec{\theta}_{noise}(\tau)\right\|\right) \tag{41}$$

and

$$\int_{t_0}^{t}\left[y_{oi}(\tau) - y_{od}^i(\tau)\right]^2 d\tau \le \frac{1}{\beta_{44}}\left[\beta_{55}\left(\left\|\vec{x}_{e0}\right\|\right) + \int_{t_0}^{t}\beta_{33}\left(\left\|\vec{\theta}_{noise}(\tau)\right\|^2\right)d\tau\right] \tag{42}$$

where t_0 is initial time, $\vec{x}(t_0)$ denotes the initial state, β_{22} and β_{44} are positive constants, β_{11} is a KL-class function, and β_{33}, β_{55} are K-class functions.

We immediately propose significant contribution for simultaneously satisfying the almost disturbance decoupling, controllable convergence rate, selecting parameter optimization, the input amplitude reduction and globally exponential stability multi-performances as follows.

Theorem 1. Exists a Lyapunov function $V_{non}: \Re^{n-r} \to \Re^+$ for transformed nonlinear subsystem such that three conditions hold for all $\vec{\eta} \in \Re^{n-r_o}$:

(a)

$$\omega_{non1}\left\|\vec{\eta}\right\|^2 \le V_{non}(\vec{\eta}) \le \omega_{non2}\left\|\vec{\eta}\right\|^2, \omega_{non1}, \omega_{non2} > 0 \tag{43}$$

(b)

$$\nabla_t V_{non} + (\nabla_{\vec{\eta}} V_{non})^T \vec{\rho}_{non}(t, \vec{\eta}, 0) \le -8\alpha_x V_{non}(\vec{\eta}), \quad \alpha_x > 0 \tag{44}$$

(c)

$$\left\|\nabla_{\vec{\eta}} V_{non}\right\| \le \varpi_{non}\left\|\vec{\eta}\right\|, \varpi_{non} > 0 \tag{45}$$

Then the LQR optimal problem using PSO algorithm with almost disturbance decoupling, controllable convergence rate, selecting parameter optimization and the input amplitude reduction multi-performances is achievable by the following input

$$\vec{u} = A^{-1}\{-\vec{u}_b + \vec{u}_v + \vec{v}_{LQR}\} \tag{46}$$

$$\vec{v}_{LQR} \equiv \left[\vec{v}_{LQR1} \cdots \vec{v}_{LQRm}\right]^T \tag{47}$$

$$J = \frac{1}{2}\int_{t_0}^{T_f}\left(\overline{e^i}^T Q \overline{e^i} + (\vec{v}_{LQRi})^T R(\vec{v}_{LQRi})\right)dt, \quad Q > 0, R > 0 \tag{48}$$

$$\vec{B}_{r_{oi}} \equiv \left[0 \cdots 0\ 1\right] \in \Re^{r_{oi} \times 1} \tag{49}$$

$$(\varepsilon^{-1}A_C^i)^T S^i + S^i(\varepsilon^{-1}A_C^i) - S^i(\varepsilon^{r_{oi}-1}\vec{B}_{r_{oi}})R^{-1}(\varepsilon^{r_{oi}-1}\vec{B}_{r_{oi}})^T S^i + Q = 0 \tag{50}$$

$$K^i = R^{-1}(\varepsilon^{r_{oi}-1}\vec{B}_{r_{oi}})S^i \equiv \left[K_{i1} \cdots K_{ir_{oi}}\right], \quad i = 1, 2, \cdots, m \tag{51}$$

$$K_{\max}^i \equiv \max\left\{K_{i1}, K_{i2}, \cdots, K_{ir_{oi}}\right\}, i = 1, 2, \cdots, m \tag{52}$$

$$\vec{u}_b \equiv \left[u_{b1}\ u_{b2} \cdots u_{bm}\right]^T \equiv \left[L_{\vec{f}}^{r_{o1}} h_{o1}\ L_{\vec{f}}^{r_{o2}} h_{o2} \cdots L_{\vec{f}}^{r_{om}} h_{om}\right]^T \tag{53}$$

$$\vec{u}_v \equiv \left[u_{v1}\ u_{v2} \cdots u_{vm}\right]^T$$

$$u_{vi} \equiv y_d^{i\,(r_{oi})} - \varepsilon^{-r_{oi}}\alpha_1^i\left[L_f^0 h_{oi}(\vec{X}) - y_{od}^i\right] - \varepsilon^{1-r_{oi}}\alpha_2^i\left[L_f^1 h_{oi}(\vec{X}) - y_{od}^{i\,(1)}\right] - \cdots - \varepsilon^{-1}\alpha_{r_{oi}}^i\left[L_f^{r_{oi}-1} h_{oi}(\vec{X}) - y_{od}^{i\,(r_{oi}-1)}\right] \tag{54}$$

$$\vec{v}_{LQRi} = -K^i\overline{e^i} \equiv -\left[K_{i1} \cdots K_{ir_{oi}}\right]\left[\overline{e_1^i}\ \overline{e_2^i} \cdots \overline{e_{r_{oi}}^i}\right]^T = -K_{i1}\overline{e_1^i} - K_{i2}\overline{e_2^i} - \cdots - K_{ir_{oi}}\overline{e_{r_{oi}}^i}, i = 1, 2, \cdots, m \tag{55}$$

and the output tracking errors can be depressed by tuning the factor $NN_2 > 1$:

$$H(\varepsilon) \equiv \begin{bmatrix} H_{11} & H_{12} \\ H_{12} & H_{22} \end{bmatrix} \tag{56}$$

$$H_{11} = 8\alpha_x - \frac{81}{18}\frac{\omega_{non3}^2}{\omega_{non1}}\left\|\phi_{\vec{\eta}}\right\|^2 \tag{57}$$

$$H_{12} = -\left[\frac{w_{bon3}M_{non}}{\sqrt{2k(\varepsilon)w_{non1}\nabla_{\min}^*}}\right] \tag{58}$$

$$H_{22} = \frac{1}{\varepsilon\nabla_{\max}^*} - \frac{K_{\max}^1\varepsilon^{r_{o1}-1}\left\|\vec{B}_{r_{o1}}^T P^1\right\|}{1/2\nabla_{\min}(P^1)} - \cdots - \frac{K_{\max}^m\varepsilon^{r_{om}-1}\left\|\vec{B}_{r_{om}}^T P^m\right\|}{1/2\nabla_{\min}(P^m)}$$

$$-\left(\frac{81}{18}\right)\frac{k(\varepsilon)\left\|\phi^1_{\vec{\xi}}\right\|^2\|P^1\|^2}{1/2\varepsilon^2\nabla_{\min}(P^1)} - \cdots - \left(\frac{81}{18}\right)\frac{k(\varepsilon)\left\|\phi^m_{\vec{\xi}}\right\|^2\|P^m\|^2}{1/2\varepsilon^2\nabla_{\min}(P^m)} \tag{59}$$

$$\alpha_s(\varepsilon) \equiv \frac{H_{11}+H_{22}-\left[(H_{11}-H_{22})^2+4H_{12}^2\right]^{1/2}}{4} \tag{60}$$

$$N \equiv 2\alpha_s(\varepsilon) \tag{61}$$

$$N_1 \equiv \frac{m+1}{18}\left(\sup_{t_0\le\tau\le t}\left\|\vec{\theta}\right\|\right)^2 \tag{62}$$

$$N_2 \equiv \min\left\{\omega_{non1}, \frac{k(\varepsilon)}{2}\nabla^*_{\min}\right\} \tag{63}$$

$$\phi^i_{\vec{\xi}}(\varepsilon) \equiv \begin{bmatrix} \varepsilon\left(\frac{\partial}{\partial\vec{X}}h_{oi}\right)\vec{q}^*_1 & \cdots & \varepsilon\left(\frac{\partial}{\partial\vec{X}}h_{oi}\right)\vec{q}^*_p \\ \vdots & & \vdots \\ \varepsilon^{r_{oi}}\left(\frac{\partial}{\partial\vec{X}}L_f^{r_{oi}-1}h_{oi}\right)\vec{q}^*_1 & \cdots & \varepsilon^{r_{oi}}\left(\frac{\partial}{\partial\vec{X}}L_f^{r_{oi}-1}h_{oi}\right)\vec{q}^*_p \end{bmatrix} \tag{64}$$

$$\phi_{\vec{\eta}}(\varepsilon) \equiv \begin{bmatrix} \left(\frac{\partial}{\partial\vec{X}}\phi_{r_o+1}\right)\vec{q}^*_1 & \cdots & \left(\frac{\partial}{\partial\vec{X}}\phi_{r_o+1}\right)\vec{q}^*_p \\ \vdots & & \vdots \\ \left(\frac{\partial}{\partial\vec{X}}\phi_n\right)\vec{q}^*_1 & \cdots & \left(\frac{\partial}{\partial\vec{X}}\phi_n\right)\vec{q}^*_p \end{bmatrix} \tag{65}$$

where H possesses positive definite property and the continuous function $k(\varepsilon):\Re^+\to\Re^+$ satisfies $\lim_{\varepsilon\to 0}k(\varepsilon)=0$ and

$$\lim_{\varepsilon\to 0}\frac{\varepsilon}{k(\varepsilon)}=0 \tag{66}$$

Moreover, the convergence rate formula of the output tracking error is firstly given to be

$$\frac{NN_2}{\Delta_{\max}} \tag{67}$$

with the globally exponential stability, where

$$\Delta_{\max} \equiv \max\left\{\omega_{non2}, \frac{k}{2}\nabla^*_{\max}\right\} \tag{68}$$

and the output tracking error of control system (8) is exponentially attracted into a ball $B_{\underline{r}}$, $\underline{r}=\sqrt{\frac{N_1}{NN_2}}$

Proof. Based on the (14)∼(16), the function ϕ defined as (18)∼(20) is a bijective and infinitely continuous function and then one can apply it to yield the following partially linear and partially nonlinear transformations

$$\begin{aligned}\dot{\xi}^1_1 &= \frac{\partial h_{o1}}{\partial\vec{X}}\left[\vec{f}+\underset{\sim}{g}\cdot\vec{u}+\sum_{j=1}^{p}\vec{q}^*_j\theta_j\right]\\ &= \xi^1_2+\sum_{j=1}^{p}\left(\frac{\partial h_{o1}}{\partial\vec{X}}\vec{q}^*_j\right)\theta_j\end{aligned} \tag{69}$$

$$\vdots$$

$$\begin{aligned}\dot{\xi}^1_{r_1-1} &= \frac{\partial L_f^{r_{o1}-2}h_{o1}}{\partial\vec{X}}\left[\vec{f}+\underset{\sim}{g}\cdot\vec{u}+\sum_{j=1}^{p}\vec{q}^*_j\theta_j\right]\\ &= \xi^1_{r_{o1}}+\sum_{j=1}^{p}\left(\frac{\partial L_f^{r_{o1}-2}h_{o1}}{\partial\vec{X}}\vec{q}^*_j\right)\theta_j\end{aligned} \tag{70}$$

$$\begin{aligned}\dot{\xi}^1_{r_1} &= \frac{\partial\phi^1_{r_{o1}}}{\partial\vec{X}}\frac{d\vec{X}}{dt}\\ &= \frac{\partial L_f^{r_{o1}-1}h_{o1}}{\partial\vec{X}}\left[\vec{f}+\underset{\sim}{g}\cdot\vec{u}+\sum_{j=1}^{p}\vec{q}^*_j\theta_j\right]\\ &= L^{r_{o1}}_{\vec{f}}h_{o1}+L_{\vec{g}_1}L^{r_{o1}-1}_{\vec{f}}h_{o1}\,u_1+\cdots\\ &\quad +L_{\vec{g}_m}L^{r_{o1}-1}_{\vec{f}}h_{o1}\,u_m\\ &\quad +\sum_{j=1}^{p}\left(\frac{\partial L_f^{r_{o1}-1}h_{o1}}{\partial\vec{X}}\vec{q}^*_j\right)\theta_j\end{aligned} \tag{71}$$

$$\vdots$$

$$\begin{aligned}\dot{\xi}^m_1 &= \frac{\partial h_{om}}{\partial\vec{X}}\left[\vec{f}+\underset{\sim}{g}\cdot\vec{u}+\sum_{j=1}^{p}\vec{q}^*_j(\theta_j)\right]\\ &= \xi^m_2+\sum_{j=1}^{p}\left(\frac{\partial h_{om}}{\partial\vec{X}}\vec{q}^*_j(\theta_j)\right)\end{aligned} \tag{72}$$

$$\vdots$$

$$\begin{aligned}\dot{\xi}^m_{r_{om}-1} &= \frac{\partial L_f^{r_{om}-2}h_{om}}{\partial\vec{X}}\left[\vec{f}+\underset{\sim}{g}\cdot\vec{u}+\sum_{j=1}^{p}\vec{q}^*_j(\theta_j)\right]\\ &= \xi^1_{r_{o1}}+\sum_{j=1}^{p}\left(\frac{\partial L_f^{r_{om}-2}h_{om}}{\partial\vec{X}}\vec{q}^*_j\right)(\theta_j)\end{aligned} \tag{73}$$

$$\begin{aligned}\dot{\xi}^m_{r_{om}} &= \frac{\partial L_f^{r_{om}-1}h_{om}}{\partial\vec{X}}\left[\vec{f}+\underset{\sim}{g}\cdot\vec{u}+\sum_{j=1}^{p}\vec{q}^*_j(\theta_j)\right]\\ &= L^{r_{om}}_{\vec{f}}h_{om}+L_{\vec{g}_1}L^{r_{om}-1}_{\vec{f}}h_{om}\,u_1+\cdots\end{aligned}$$

$$+L_{\vec{g}_m} L_{\vec{f}}^{r_{om}-1} h_{om}\, u_m + \sum_{j=1}^{p} \left(\frac{\partial L_f^{r_{om}-1} h_{om}}{\partial \vec{X}} \vec{q}_j^{\,*} \right) (\theta_j) \tag{74}$$

$$\dot{\vec{\eta}}_k = \frac{\partial \phi_k}{\partial \vec{X}} \left[\vec{f} + \underset{\sim}{g} \cdot \vec{u} + \sum_{j=1}^{p} \vec{q}_j^{\,*} (\theta_j) \right] = q_k + \sum_{j=1}^{p} \left(\frac{\partial \phi_k}{\partial \vec{X}} \vec{q}_j^{\,*} \right) (\theta_j) \tag{75}$$

Since

$$u_{ci}(\vec{\xi}, \vec{\eta}) \equiv L_{\vec{f}}^{r_{io}} h_{oi}(\vec{X}(t)) \tag{76}$$

$$u_{dij} \equiv L_{\vec{g}_j} L_{\vec{f}}^{r_{oi}-1} h_{oi}(\vec{X}),\ 1 \le i, j \le m \tag{77}$$

$$\vec{\rho}_k(\vec{\xi}, \vec{\eta}) = L_{\vec{f}} \varphi_k(\vec{X}),\ k = r_o + 1, r_o + 2, \cdots, n \tag{78}$$

the dynamic equations of control system (8) can be described with new transformed states as

$$\dot{\xi}_i^1(t) = \xi_{i+1}^1(t) + \sum_{j=1}^{p} \left(\frac{\partial}{\partial \vec{X}} L_{\vec{f}}^{i-1} h_{o1} \right) \vec{q}_j^{\,*} (\theta_j),\quad i = 1, 2, \cdots, r_{o1} - 1 \tag{79}$$

$$\dot{\xi}_{r_{o1}}^1 = u_{c1}(\vec{\xi}, \vec{\eta}) + u_{d11}(\vec{\xi}, \vec{\eta}) u_1 + \cdots + u_{d1m}(\vec{\xi}, \vec{\eta}) u_m + \sum_{j=1}^{p} \left(\frac{\partial}{\partial \vec{X}} L_{\vec{f}}^{r_{o1}-1} h_{o1} \right) \vec{q}_j^{\,*} (\theta_j) \tag{80}$$

$$\vdots$$

$$\dot{\xi}_i^m = \xi_{i+1}^m + \sum_{j=1}^{p} \left(\frac{\partial}{\partial \vec{X}} L_{\vec{f}}^{i-1} h_{om} \right) \vec{q}_j^{\,*} (\theta_j),\quad i = 1, 2, \cdots, r_{om} - 1 \tag{81}$$

$$\dot{\xi}_{r_{om}}^m = u_{cm}(\vec{\xi}, \vec{\eta}) + u_{dm1}(\vec{\xi}, \vec{\eta}) u_1 + \cdots + u_{dmm}(\vec{\xi}, \vec{\eta}) u_m + \sum_{j=1}^{p} \left(\frac{\partial}{\partial \vec{X}} L_{\vec{f}}^{r_{om}-1} h_{om} \right) \vec{q}_j^{\,*} (\theta_j) \tag{82}$$

$$\dot{\vec{\eta}}_k = \vec{\rho}_k(\vec{\xi}, \vec{\eta}) + \sum_{j=1}^{p} \left(\frac{\partial}{\partial \vec{X}} \phi_k(\vec{X}) \right) \vec{q}_j^{\,*} (\theta_j),\quad k = r_o + 1, \cdots, n \tag{83}$$

$$y_{oi} = \xi_1^i,\ 1 \le i \le m \tag{84}$$

In this study, the desired inputs are constructed by the virtual input $\vec{u}_b \equiv \left[L_{\vec{f}}^{r_{o1}} h_{o1}\ L_{\vec{f}}^{r_{o2}} h_{o2} \cdots L_{\vec{f}}^{r_{om}} h_{om} \right]^T$, part input $\vec{u}_v \equiv \left[u_{v1}\ u_{v2} \cdots u_{vm} \right]^T$ and the LQR part input $\vec{v}_{LQR}$ using PSO, and are mainly combined to simultaneously achieve almost disturbance decoupling performance, input amplitude reduction performance and controllable convergent rate performance, respectively. From (55)(76) and (77), the hybrid control can be described as

$$\vec{u} = A^{-1} \{ -\vec{u}_b + \vec{u}_v + \vec{v}_{LQR} \} \tag{85}$$

Substituting (85) into (80) and (82), the dynamic equations of system (8) can be derived as:

$$\begin{bmatrix} \dot{\xi}_1^i \\ \dot{\xi}_2^i \\ \vdots \\ \dot{\xi}_{r_{oi}-1}^i \\ \dot{\xi}_{r_{oi}}^i \end{bmatrix} = \begin{bmatrix} 0 & 1 & 0 & \cdots & 0 \\ 0 & 0 & 1 & 0 \cdots & 0 \\ & \vdots & & & \vdots \\ 0 & 0 & 0 & \cdots & 1 \\ 0 & 0 & 0 & \cdots & 0 \end{bmatrix} \begin{bmatrix} \xi_1^i \\ \xi_2^i \\ \vdots \\ \xi_{r_{oi}-1}^i \\ \xi_{r_{oi}}^i \end{bmatrix} + \begin{bmatrix} 0 \\ 0 \\ \vdots \\ 0 \\ 1 \end{bmatrix} \left(u_{vi} + v_{LQRi} \right) + \begin{bmatrix} \sum_{j=1}^{p} \left(\frac{\partial}{\partial \vec{X}} h_{oi} \right) \left(\vec{q}_j^{\,*} (\theta_j) \right) \\ \sum_{j=1}^{p} \left(\frac{\partial}{\partial \vec{X}} L_{\vec{f}}^{1} h_{oi} \right) \left(\vec{q}_j^{\,*} (\theta_j) \right) \\ \vdots \\ \sum_{j=1}^{p} \left(\frac{\partial}{\partial \vec{X}} L_f^{r_{oi}-1} h_{oi} \right) \left(\vec{q}_j^{\,*} (\theta_j) \right) \end{bmatrix} \tag{86}$$

$$\left[\dot{\eta}_{r_o+1} \cdots \dot{\eta}_n(t) \right]^T = \left[\rho_{r_o+1} \cdots \rho_n \right]^T + \left[\sum_{j=1}^{p} \left(\frac{\partial}{\partial \vec{X}} \phi_{r_o+1} \right) \left(\vec{q}_j^{\,*} (\theta_j) \right) \cdots \sum_{j=1}^{p} \left(\frac{\partial}{\partial \vec{X}} \phi_n \right) \left(\vec{q}_j^{\,*} (\theta_j) \right) \right]^T \tag{87}$$

$$y_{oi} = \xi_1^i \tag{88}$$

Stabilization and tracking problems are significant subjects for nonlinear control theory. Tracking problem is generally more complex than stabilization problem for nonlinear control systems. In order to convert the tracking problem to stabilization problem, we apply parameters e_j^i, $\overline{e_j^i}$, $\overline{e^i}$, $\bar{e}$ to track the desired signals $y_{od}^{i(j-1)}$. Applying (21)(23)(24)(29) and (55) converts (86)∼(88) to be

$$\dot{\vec{\eta}} = \vec{\rho}(\vec{\xi}, \vec{\eta}) + \phi_{\vec{\eta}} \left(\vec{\theta} \right) \equiv \vec{\rho}_{non}(t, \vec{\eta}, \bar{e}) + \phi_{\vec{\eta}} \left(\vec{\theta} \right) \tag{89}$$

$$\varepsilon \dot{\overline{e^i}} = A_c^i \overline{e^i} + \vec{B}_{r_{oi}} \left(\varepsilon^{r_{oi}} \vec{v}_{LQRi} \right) + \phi_\xi^i \left(\vec{\theta} \right) \tag{90}$$

$$y_{oi} = \xi_1^i \tag{91}$$

Applying the linear quadratic regulator approach with PSO algorithm obtains

$$\vec{v}_{LQR} \equiv \left[\vec{v}_{LQR1} \cdots \vec{v}_{LQRm}\right]^T \tag{92}$$

$$\begin{aligned}\vec{v}_{LQRi} &= -K^i\overline{e^i} \equiv -\left[K_{i1} \cdots K_{ir_{oi}}\right]\left[\overline{e_1^i}\ \overline{e_2^i} \cdots \overline{e_{r_{oi}}^i}\right]^T \\ &= -K_{i1}\overline{e_1^i} - K_{i2}\overline{e_2^i} - \cdots - K_{ir_{oi}}\overline{e_{r_{oi}}^i}, \\ i &= 1, 2, \cdots, m\end{aligned} \tag{93}$$

$$\vec{B}_{r_{oi}} \equiv \left[0 \cdots 0\ 1\right] \in \Re^{r_{oi}\times 1} \tag{94}$$

$$\begin{aligned}K^i &= R^{-1}(\varepsilon^{r_{oi}-1}\vec{B}_{r_{oi}})S^i \equiv \left[K_{i1} \cdots K_{ir_{oi}}\right], \\ i &= 1, 2, \cdots, m\end{aligned} \tag{95}$$

$$K^i_{\max} \equiv \max\left\{K_{i1}, K_{i2}, \cdots, K_{ir_{oi}}\right\}, \quad i=1, 2, \cdots, m \tag{96}$$

with the performance cost index

$$J = \frac{1}{2}\int_{t_0}^{T_f}\left(\overline{e^i}^T Q\overline{e^i} + (\vec{v}_{LQRi})^T R(\vec{v}_{LQRi})\right)dt \tag{97}$$

and the algebraic Riccati equation

$$\begin{aligned}&(\varepsilon^{-1}A_C^i)^T S^i + S^i(\varepsilon^{-1}A_C^i) \\ &\quad - S^i(\varepsilon^{r_{oi}-1}\vec{B}_{r_{oi}})R^{-1}(\varepsilon^{r_{oi}-1}\vec{B}_{r_{oi}})^T S^i + Q = 0\end{aligned} \tag{98}$$

For the new dynamic equations, a composite Lyapunov function $V_{com}\left(\bar{e}, \vec{\eta}\right)$ is constructed to be sum of Lyapunov functions $V_{non}(\vec{\eta})$ and $W(\bar{e})$ for nonlinear subsystem and linear subsystem, respectively [66],

$$V_{com}\left(\bar{e}, \vec{\eta}\right) \equiv V_{non}(\vec{\eta}) + k(\varepsilon)W(\bar{e}) \tag{99}$$

where $W(\bar{e})$ is defined to be

$$W(\bar{e}) = W^1\left(\overline{e^1}\right) + \cdots + W^m\left(\overline{e^m}\right) \tag{100}$$

and

$$W^i\left(\overline{e^i}\right) \equiv \frac{1}{2}\overline{e^i}^T P^i\overline{e^i} \tag{101}$$

Using (21)(36)(43)(44) and (45) yields the derivative of the composite Lyapunov function

$$\begin{aligned}&\dot{V}_{com} \\ &= \left[\nabla_t V_{non} + \left(\nabla_{\vec{\eta}} V_{non}\right)^T \dot{\vec{\eta}}\right] \\ &\quad + \frac{k}{2}\left[\left(\dot{\overline{e^1}}\right)^T P^1\overline{e^1} + \left(\overline{e^1}\right)^T P^1\left(\dot{\overline{e^1}}\right) + \cdots\right. \\ &\quad \left. + \left(\dot{\overline{e^m}}\right)^T P^m\overline{e^m} + \left(\overline{e^m}\right)^T P^m\left(\dot{\overline{e^m}}\right)\right] \\ &= \left[\nabla_t V_{non} + \left(\nabla_{\vec{\eta}} V_{non}\right)^T\left(\vec{\rho}_{non}(t, \vec{\eta}, \bar{e}) + \phi_{\vec{\eta}}\left(\vec{\theta}\right)\right)\right] \\ &\quad + \left\{\frac{k}{2\varepsilon}\left(\overline{e^1}\right)^T\left[P^1\left(A_c^1\right) + \left(A_c^1\right)^T P^1\right]\overline{e^1} + \cdots\right. \\ &\quad \left. + \frac{k}{2\varepsilon}\left(\overline{e^m}\right)^T\left[P^m\left(A_c^m\right) + \left(A_c^m\right)^T P^m\right]\overline{e^m}\right. \\ &\quad \left. + \frac{k}{\varepsilon}\left\{\left(\vec{\theta}\right)^T\left[\left(\phi_\xi^1\right)^T P^1\overline{e^1} + \cdots + \left(\phi_\xi^m\right)^T P^m\overline{e^m}\right]\right\}\right. \\ &\quad \left. + \left[k\varepsilon^{r_{o1}-1}\vec{B}_{r_{o1}}^T P^1\overline{e^1}v_{LQR1}\right.\right. \\ &\quad \left.\left. + \cdots + k\varepsilon^{r_{om}-1}\vec{B}_{r_{om}}^T P^m\overline{e^m}v_{LQRm}\right]\right\} \\ &\le \left[\nabla_t V_{non} + \left(\nabla_{\vec{\eta}} V_{non}\right)^T\vec{\rho}_{non}(t, \vec{\eta}, \bar{e})\right. \\ &\quad \left. + \left\|\nabla_{\vec{\eta}} V_{non}\right\|\left\|\phi_{\vec{\eta}}\right\|\left\|\left(\vec{\theta}\right)\right\|\right] \\ &\quad - \frac{k}{2\varepsilon}\left[\left\|\overline{e^1}\right\|^2 + \cdots + \left\|\overline{e^m}\right\|^2\right] \\ &\quad + \frac{k}{\varepsilon}\left[\left\|\left(\vec{\theta}\right)\right\|\left(\left\|\phi_\xi^1\right\|\left\|P^1\right\|\left\|\overline{e^1}\right\|\right.\right. \\ &\quad \left.\left. + \cdots + \left\|\phi_\xi^m\right\|\left\|P^m\right\|\left\|\overline{e^m}\right\|\right)\right] \\ &\quad + k\varepsilon^{r_{o1}-1}\left\|\vec{B}_{r_{o1}}^T P^1\right\|\left\|\overline{e^1}\right\|\left\|v_{LQR1}\right\| \\ &\quad + \cdots + k\varepsilon^{r_{om}-1}\left\|\vec{B}_{r_{om}}^T P^m\right\|\left\|\overline{e^m}\right\|\left\|v_{LQRm}\right\| \\ &\le \left[\nabla_t V_{non} + \left(\nabla_{\vec{\eta}} V_{non}\right)^T\vec{\rho}_{non}(t, \vec{\eta}, 0)\right] \\ &\quad - \left(\nabla_{\vec{\eta}} V_{non}\right)^T\vec{\rho}_{non}(t, \vec{\eta}, 0) \\ &\quad + \left(\nabla_{\vec{\eta}} V_{non}\right)^T\vec{\rho}_{non}(t, \vec{\eta}, \bar{e}) \\ &\quad + \left\|\nabla_\eta V\right\|\left\|\phi_\eta\right\|\left\|\vec{\theta}\right\| - \frac{k}{\varepsilon}\left[\frac{W^1}{\nabla_{\max}(P^1)} + \cdots + \frac{W^m}{\nabla_{\max}(P^m)}\right] \\ &\quad + \frac{81}{18}\frac{k^2}{\varepsilon^2}\left\|\phi_\xi^1\right\|^2\left\|P^1\right\|^2\left\|\overline{e^1}\right\|^2 + \frac{1}{18}\left\|\vec{\theta}\right\|^2 + \cdots \\ &\quad + \frac{81}{18}\frac{k^2}{\varepsilon^2}\left\|\phi_\xi^m\right\|^2\left\|P^m\right\|^2\left\|\overline{e^m}\right\|^2 + \frac{1}{18}\left\|\vec{\theta}\right\|^2 \\ &\quad + k\varepsilon^{r_{o1}-1}\left\|\vec{B}_{r_{o1}}^T P^1\right\|\left\|\overline{e^1}\right\|K^1_{\max}\left\|\overline{e^1}\right\| + \cdots \\ &\quad + k\varepsilon^{r_{om}-1}\left\|\vec{B}_{r_{om}}^T P^m\right\|\left\|\overline{e^m}\right\|K^m_{\max}\left\|\overline{e^m}\right\| \\ &\le -8\alpha_x V_{non} + \omega_{non3}\left\|\vec{\eta}\right\|M_{non}\left\|\bar{e}\right\| + \omega_{non3}\left\|\vec{\eta}\right\|\left\|\phi_\eta\right\|\left\|\vec{\theta}\right\| \\ &\quad - \frac{k}{\varepsilon}\frac{1}{\nabla^*_{\max}}W + \frac{81}{18}\frac{k^2}{\varepsilon^2}\left\|\phi_\xi^1\right\|^2\left\|P^1\right\|^2\left\|\overline{e^1}\right\|^2 + \frac{1}{18}\left\|\vec{\theta}\right\|^2 \\ &\quad + \cdots + \frac{81}{18}\frac{k^2}{\varepsilon^2}\left\|\phi_\xi^m\right\|^2\left\|P^m\right\|^2\left\|\overline{e^m}\right\|^2 + \frac{1}{18}\left\|\vec{\theta}\right\|^2 \\ &\quad + K^1_{\max}k\varepsilon^{r_{o1}-1}\left\|\vec{B}_{r_{o1}}^T P^1\right\|\left\|\overline{e^1}\right\|^2 \\ &\quad + \cdots + K^m_{\max}k\varepsilon^{r_{om}-1}\left\|\vec{B}_{r_{om}}^T P^m\right\|\left\|\overline{e^m}\right\|^2 \\ &\le -\left(8\alpha_x - \frac{81}{18}\left(\frac{\omega_{non3}}{\sqrt{\omega_{non1}}}\left\|\phi_{\vec{\eta}}\right\|\right)^2\right)\left(\sqrt{V_{non}}\right)^2 \\ &\quad + 2\left(\frac{\omega_{non3}M_{non}}{\sqrt{2\omega_{non1}k\nabla^*_{\min}}}\right)\sqrt{V_{non}}\sqrt{kW}\end{aligned}$$

$$
\begin{aligned}
&-\left(\frac{1}{\varepsilon\nabla^*_{\max}}-\frac{81}{18}\frac{k\left\|\phi^1_\xi\right\|^2\left\|P^1\right\|^2}{1/2\varepsilon^2\nabla_{\min}(P^1)}\right.\\
&\left.-\frac{K^1_{\max}\varepsilon^{r_{o1}-1}\left\|\vec{B}^T_{r_{o1}}P^1\right\|}{1/2\nabla_{\min}(P^1)}-\cdots\right.\\
&-\left(\frac{1}{\varepsilon\nabla^*_{\max}}-\frac{81}{18}\frac{k\left\|\phi^1_\xi\right\|^2\left\|P^1\right\|^2}{1/2\varepsilon^2\nabla_{\min}(P^1)}\right.\\
&\left.-\frac{K^1_{\max}\varepsilon^{r_{o1}-1}\left\|\vec{B}^T_{r_{o1}}P^1\right\|}{1/2\nabla_{\min}(P^1)}-\cdots\right.\\
&=-\left[\sqrt{V_{non}}\ \sqrt{kW}\right]H\left[\begin{array}{c}\sqrt{V_{non}}\\ \sqrt{kW}\end{array}\right]+\frac{m+1}{18}\left\|\vec{\theta}\right\|^2 \qquad (102)
\end{aligned}
$$

i.e.

$$
\dot{V}_{com}\le-\nabla_{\min}(H)V_{com}+\frac{m+1}{18}\left\|\vec{\theta}\right\|^2 \qquad (103)
$$

where $\nabla_{\min}(H)$ is the minimum eigenvalue of the matrix H. From (60), we get

$$
\nabla_{\min}(H)=2\alpha_s \qquad (104)
$$

Applying $\nabla_{\min}(H)=2\alpha_s$ into (103) yields

$$
\begin{aligned}
\dot{V}_{com}&\le-2\alpha_sV_{com}+\frac{m+1}{18}\left\|\vec{\theta}\right\|^2\\
&\le-NN_2\left(\left\|\vec{\eta}\right\|^2+\|\bar{e}\|^2\right)+\frac{m+1}{18}\left\|\vec{\theta}\right\|^2 \qquad (105)
\end{aligned}
$$

Let

$$
\bar{e}\equiv\left[\overline{e^1}\ \cdots\ \overline{e^m}\right]^T\equiv\left[\overline{e^1_1}\ \overline{e^1_{rem}}\right]^T,\ \overline{e^1_{rem}}\in\Re^{r_o-1} \qquad (106)
$$

Hence

$$
\dot{V}_{com}\le-NN_2\left(\left\|\vec{\eta}\right\|^2+\left\|\overline{e^1_1}\right\|^2+\left\|\overline{e^1_{rem}}\right\|^2\right)+\frac{m+1}{18}\left\|\vec{\theta}\right\|^2 \qquad (107)
$$

Then

$$
\int_{t_0}^{t}\left(y_{o1}(\tau)-y^1_{od}(\tau)\right)^2d\tau\le\frac{V_{com}(t_0)}{NN_2}+\frac{m+1}{18NN_2}\int_{t_0}^{t}\left\|\vec{\theta}\right\|^2d\tau \qquad (108)
$$

It is easy to similarly derive that

$$
\begin{aligned}
&\int_{t_0}^{t}\left(y_{oi}(\tau)-y^i_{od}(\tau)\right)^2d\tau\\
&\le\frac{V_{non}(t_0)}{NN_2}+\frac{m+1}{18NN_2}\int_{t_0}^{t}\left\|\vec{\theta}\right\|^2d\tau,\quad 2\le i\le m \qquad (109)
\end{aligned}
$$

so that third almost disturbance decoupling condition (42) is satisfied. From (105), we obtain

$$
\dot{V}_{com}\le-NN_2\left(\left\|\vec{y}_{o-total}\right\|^2\right)+\frac{m+1}{18}\left\|\vec{\theta}\right\|^2 \qquad (110)
$$

where

$$
\left\|\vec{y}_{o-total}\right\|^2\equiv\|\bar{e}\|^2+\left\|\vec{\eta}\right\|^2 \qquad (111)
$$

Applying the input-to-state stable theorem [65] yields the input-to-state stability for the desired control system for first almost disturbance decoupling condition (40). Moreover, it is easy to get

$$
\Delta_{\min}\left(\|\bar{e}\|^2+\left\|\vec{\eta}\right\|^2\right)\le V_{non}\le\Delta_{\max}\left(\|\bar{e}\|^2+\left\|\vec{\eta}\right\|^2\right) \qquad (112)
$$

i.e.

$$
\Delta_{\min}\left(\left\|\vec{y}_{o-total}\right\|^2\right)\le V_{non}\le\Delta_{\max}\left(\left\|\vec{y}_{o-total}\right\|^2\right) \qquad (113)
$$

where $\Delta_{\min}\equiv\min\left\{\omega_{non1},\frac{k}{2}\nabla^*_{\min}\right\}$ and $\Delta_{\max}\equiv\max\left\{\omega_{non2},\frac{k}{2}\nabla^*_{\max}\right\}$. Combining (62), (105) and (113) gets

$$
\dot{V}_{com}\le-\frac{NN_2}{\Delta_{\max}}V_{com}+N_1 \qquad (114)
$$

Then,

$$
V_{com}(t)\le V_{com}(t_0)e^{-\frac{NN_2}{\Delta_{\max}}(t-t_0)}+\frac{\Delta_{\max}N_1}{NN_2},\quad t\ge t_0 \qquad (115)
$$

which achieves

$$
\left|y_{o1}(t)-y^1_{od}(t)\right|\le\sqrt{\frac{2V_{non}(t_0)}{k\nabla^*_{\min}}}e^{-\frac{NN_2}{2\Delta_{\max}}(t-t_0)}+\sqrt{\frac{2\Delta_{\max}N_1}{k\nabla^*_{\min}NN_2}} \qquad (116)
$$

It is easy to similarly derive that

$$
\begin{aligned}
\left|y_{oi}(t)-y^i_{od}(t)\right|&\le\sqrt{\frac{2V_{non}(t_0)}{k\nabla^*_{\min}}}e^{-\frac{NN_2}{2\Delta_{\max}}(t-t_0)}\\
&+\sqrt{\frac{2\Delta_{\max}N_1}{k\nabla^*_{\min}NN_2}},\quad 2\le i\le m \qquad (117)
\end{aligned}
$$

So that second almost disturbance decoupling condition (41) is verified and then three strict almost disturbance decoupling conditions are simultaneously proved. Moreover, from(117), we have firstly proposed the convergence rate formula of output tracking errors to be $NN_2/2\Delta_{\max}$. We can adjust NN_2 to increase the convergence rate of the output tracking errors. Finally, we will verify that the ball $B_{\underline{r}}$ is a global attractor for the output tracking errors of the control system Eq. (8). Using (62)(105) and (111) yields

$$
\dot{V}_{com}\le-NN_2\left(\left\|\vec{y}_{o-total}\right\|^2\right)+N_1 \qquad (118)
$$

For $\left\|\vec{y}_{o-total}\right\| > \underline{r}$, we get $\dot{V}_{non} < 0$ and then any ball described by

$$B_{\underline{r}} \equiv \left\{ \begin{bmatrix} \bar{e} \\ \vec{\eta} \end{bmatrix} : \|\bar{e}\|^2 + \left\|\vec{\eta}\right\|^2 \leq \underline{r} \right\} \tag{119}$$

is a global final attractor for the output tracking errors of the control system (8). Furthermore, applying (113) and (115) gets

$$V_{com}(t) \leq V_{com}(t_0) e^{-\frac{NN_2}{\Delta_{\max}}(t-t_0)} + \frac{\Delta_{\max} N_1}{NN_2}, t \geq t_0$$

and

$$\begin{aligned} &\Delta_{\min} \left\|\vec{y}_{o-total}\right\|^2 \\ &\quad \leq V_{non} \leq V_{non}(t_0) e^{-\frac{NN_2}{\Delta_{\max}}(t-t_0)} + \frac{\Delta_{\max} N_1}{NN_2} \\ &\quad \leq \Delta_{\max} \left\|\vec{y}_{o-total}(t_0)\right\|^2 e^{-\frac{NN_2}{\Delta_{\max}}(t-t_0)} + \frac{\Delta_{\max} N_1}{NN_2} \end{aligned} \tag{120}$$

Consequently, we get

$$\begin{aligned} \left\|\vec{y}_{o-total}\right\|^2 \leq \frac{\Delta_{\max}}{\Delta_{\min}} \left\|\vec{y}_{o-total}(t_0)\right\|^2 e^{-\frac{NN_2}{\Delta_{\max}}(t-t_0)} \\ + \frac{N_1}{NN_2} \frac{\Delta_{\max}}{\Delta_{\min}} \end{aligned} \tag{121}$$

Hence we can conclude that the ball $B_{\underline{r}}$ is a global attractor for the output tracking errors of the control system (8) with globally exponential stability.

To systematically design input of achieving multi-performances with the almost disturbance decoupling, controllable convergence rate, selecting parameter optimization, the input amplitude reduction and globally exponential stability, an effective algorithm of designing key factors for Theorem 1 is shown in Fig. 2 and summarized as follows:

(Step 1)For the desired outputs $h_{o1}, \cdots, h_{om}$, calculate the vector relative degree $r_{o1}, \cdots, r_{om}$ of the dynamic equation.

(Step 2)Build a bijective and infinitely continuous function φ to meet (17).

(Step 3)Adjust factors $\alpha^i_{r_{oi}}$ according to (29) and (31), and find the solutions $P^i > 0$ of the Lyapunov equation, so that the matrices A^i_c are Hurwitz matrices via MATLAB.

(Step 4)Construct the Lyapunov function to satisfy the conditions (36)(43)∼(45) of the transformed partially nonlinear subsystem. If the system possesses full relative degree, i.e. $r_{o1} + \cdots + r_{om} = n$, then this step will be neglected and go to the next step.

(Step 5)According to (56)∼(65), design factors $K^i_{\max}, K_{ir_{oi}}, k, \alpha_s(\varepsilon), \varepsilon$ appropriately by LQR optimization approach using PSO algorithm to achieve $NN_2 > 1$. Moreover, from the convergence rate formula (60)(61)(63)(67) and (68), we can achieve LQR optimal weighting matrices Q and R using PSO algorithm to increase NN_2 and then increase the convergence rate.

(Step 6)The desired input can be designed by (46).

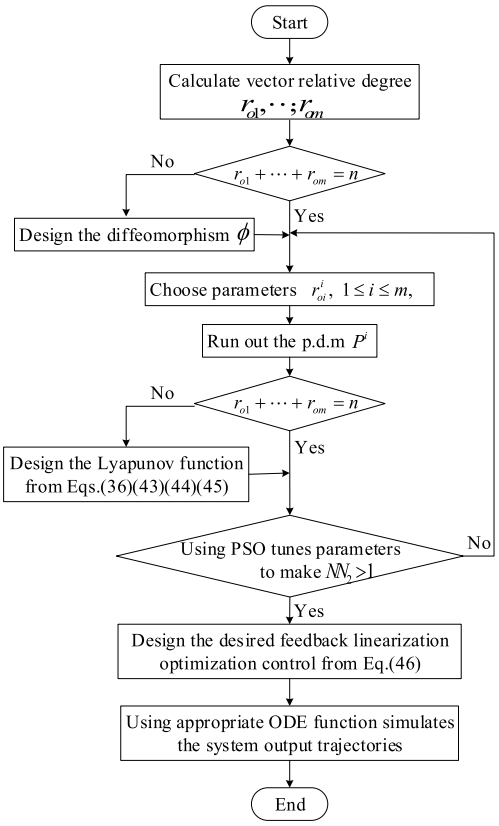

FIGURE 2. Block diagram for the effective algorithm of designing the controller.

IV. COMPOSITE FEEDBACK LINEARIZIED LQR CONTROLLER DESIGN USING PSO FOR A QUADROTOR

The quadrotor is a great platform for industrial applications as it is complex nonlinear control system. The motions along x, y axes are obtained by pitch and roll rotations for a quadrotor, respectively as shown as Fig. 1. The complete mathematical model of a quadrotor will be derived by Newton-Euler theorem with the following assumptions [67]:

(i)The aerodynamic forces and moments are assumed to be neglected.

(ii)The propellers and the quadrotor have rigid and symmetrical characteristics.

(iii)The thrust force and drag torque are proportional to the square of propeller's speed with thrust and drag factors, respectively.

(iv)The gravity center of the quadrotor is set to be the origin of the vehicle frame.

Define the vehicle-1 frame to be positively rotated by the yaw angle ψ from the vehicle frame, and then the rotation matrix from the vehicle frame to the vehicle-1 frame is derived as

$$\Re^{v1}_{v}(\psi) = \begin{bmatrix} \cos\psi & \sin\psi & 0 \\ -\sin\psi & \cos\psi & 0 \\ 0 & 0 & 1 \end{bmatrix} \tag{122}$$

The vehicle-2 frame is obtained by rotating positively the vehicle-1 frame with the pitch angle θ, and then the rotation

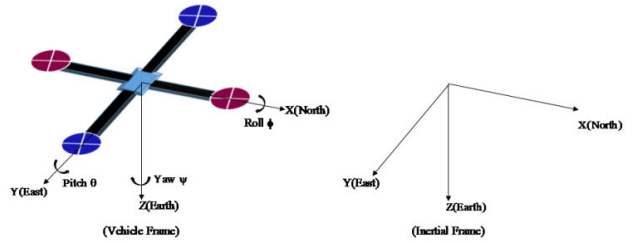

FIGURE 3. The inertial frame (earth frame) and vehicle frame for a quadrotor.

matrix from the vehicle-1 frame to the vehicle-2 frame is given by

$$\Re_{v1}^{v2}(\theta) = \begin{bmatrix} \cos\theta & 0 & -\sin\theta \\ 0 & 1 & 0 \\ \sin\theta & 0 & \cos\theta \end{bmatrix} \tag{123}$$

Let the body frame be obtained by rotating the vehicle-2 frame in right-handed rotation by the roll angle ϕ, and then the rotation matrix from the vehicle-2 frame to the body frame is formulated by

$$\Re_{v2}^{b}(\phi) = \begin{bmatrix} 1 & 0 & 0 \\ 0 & \cos\phi & \sin\phi \\ 0 & -\sin\phi & \cos\phi \end{bmatrix} \tag{124}$$

Then the complete rotation matrix from the vehicle frame to the body frame is summarized by

$$\begin{aligned} &\Re_{v}^{b}(\phi,\theta,\psi) \\ &= \Re_{v2}^{b}(\phi)\,\Re_{v1}^{v2}(\theta)\,\Re_{v}^{v1}(\psi) \\ &= \begin{bmatrix} 1 & 0 & 0 \\ 0 & \cos\phi & \sin\phi \\ 0 & -\sin\phi & \cos\phi \end{bmatrix} \begin{bmatrix} \cos\theta & 0 & -\sin\theta \\ 0 & 1 & 0 \\ \sin\theta & 0 & \cos\theta \end{bmatrix} \\ &\quad \times \begin{bmatrix} \cos\psi & \sin\psi & 0 \\ -\sin\psi & \cos\psi & 0 \\ 0 & 0 & 1 \end{bmatrix} \\ &= \begin{bmatrix} c\theta c\psi & c\theta s\psi & -s\theta \\ s\phi s\theta c\psi - c\phi s\psi & s\phi s\theta s\psi + c\phi c\psi & s\phi c\theta \\ c\phi s\theta c\psi + s\phi s\psi & c\phi s\theta s\psi - s\phi c\psi & c\phi c\theta \end{bmatrix} \end{aligned} \tag{125}$$

where s and c operators denote $s \equiv \sin$ and $c \equiv \cos$ functions, respectively.

To achieve good control performance of a quadrotor, the kinematics and the dynamic equations of the quadrotor are derived as follows. The linear velocities $(\dot{x}, \dot{y}, \dot{z})$ are inertial frame quantities, whereas (u, v, ω) are body frame quantities. Then the rotation relationship between both quantities is related by

$$\begin{aligned} \begin{bmatrix} \dot{x} \\ \dot{y} \\ \dot{z} \end{bmatrix} &= \Re_{v}^{b} \begin{bmatrix} u \\ v \\ \omega \end{bmatrix} = \left(\Re_{b}^{v}\right)^{-1} \begin{bmatrix} u \\ v \\ \omega \end{bmatrix} = \left(\Re_{b}^{v}\right)^{T} \begin{bmatrix} u \\ v \\ \omega \end{bmatrix} \\ &= \begin{bmatrix} c\theta c\psi & s\varphi s\theta c\psi - c\varphi s\psi & c\varphi s\theta c\psi + s\varphi s\psi \\ c\theta s\psi & s\varphi s\theta s\psi + c\varphi c\psi & c\varphi s\theta s\psi - s\varphi c\psi \\ -s\theta & s\varphi c\theta & c\varphi c\theta \end{bmatrix} \begin{bmatrix} u \\ v \\ \omega \end{bmatrix} \end{aligned} \tag{126}$$

The angle velocities (p, q, r) are expressed in body frame, whereas the roll angle velocity $\dot{\varphi}$, pitch angle velocity $\dot{\theta}$, yaw angle velocity $\dot{\psi}$ are defined in the vehile-2 frame, the vehile-1 frame and the vehicle frame, respectively. Consider $\dot{\varphi}, \dot{\theta}, \dot{\psi}$ to be small and then

$$\Re_{v2}^{b}(\dot{\varphi}) = \Re_{v1}^{v2}(\dot{\theta}) = \Re_{v}^{v1}(\dot{\psi}) = \begin{bmatrix} 1 & 0 & 0 \\ 0 & 1 & 0 \\ 0 & 0 & 1 \end{bmatrix} \tag{127}$$

Hence

$$\begin{aligned} &\begin{bmatrix} p \\ q \\ r \end{bmatrix} \\ &= \Re_{v2}^{b}(\dot{\varphi}) \begin{bmatrix} \dot{\varphi} \\ 0 \\ 0 \end{bmatrix} + \Re_{v2}^{b}(\varphi)\Re_{v1}^{v2}(\dot{\theta}) \begin{bmatrix} 0 \\ \dot{\theta} \\ 0 \end{bmatrix} \\ &\quad + \Re_{v2}^{b}(\varphi)\Re_{v1}^{v2}(\theta)\Re_{v}^{v1}(\dot{\psi}) \begin{bmatrix} 0 \\ 0 \\ \dot{\psi} \end{bmatrix} = \begin{bmatrix} \dot{\varphi} \\ 0 \\ 0 \end{bmatrix} + \Re_{v2}^{b}(\varphi) \begin{bmatrix} 0 \\ \dot{\theta} \\ 0 \end{bmatrix} \\ &\quad + \Re_{v2}^{b}(\varphi)\Re_{v1}^{v2}(\theta) \begin{bmatrix} 0 \\ 0 \\ \dot{\psi} \end{bmatrix} = \begin{bmatrix} 1 & 0 & -s\theta \\ 0 & c\varphi & s\varphi c\theta \\ 0 & -s\varphi & c\varphi c\theta \end{bmatrix} \begin{bmatrix} \dot{\varphi} \\ \dot{\theta} \\ \dot{\psi} \end{bmatrix} \end{aligned} \tag{128}$$

i.e.

$$\begin{bmatrix} \dot{\varphi} \\ \dot{\theta} \\ \dot{\psi} \end{bmatrix} = \begin{bmatrix} 1 & \sin(\varphi)\tan(\theta) & \cos(\varphi)\tan(\theta) \\ 0 & \cos(\varphi) & -\sin(\varphi) \\ 0 & \sin(\varphi)\sec(\theta) & \cos(\varphi)\sec(\theta) \end{bmatrix} \begin{bmatrix} p \\ q \\ r \end{bmatrix} \tag{129}$$

Let $\vec{v}$ and $\vec{a}$ be the velocity vector and acceleration vector, respectively. Since the Newton's second law only holds in inertial frame, using the Newton's second law yields the translational motion as

$$\vec{f} = m\vec{a} = m\frac{d\vec{v}}{dt_i} \tag{130}$$

where d/dt_i denotes the time derivative in the inertial frame, m is the mass of the quadrotor and $\vec{f}$ denotes the external force. Applying the Coriolis equation yields

$$\vec{f} = m\frac{d\vec{v}}{dt_i} = m\left(\frac{d\vec{v}}{dt_b} + \vec{\omega}_i \times \vec{v}\right) \tag{131}$$

where $\vec{\omega}_i$ denotes the angular velocity of the airframe in inertial frame and $\times$ is the cross product vector operator. Since $\vec{f}$ and $\vec{\omega}_i$ are used in the body frame, we will express the Coriolis equation in the body frame with $\vec{\omega}_b = \begin{bmatrix} p & q & r \end{bmatrix}^T$, $\vec{f}_b = \begin{bmatrix} f_x & f_y & f_z \end{bmatrix}^T$, and $\vec{v}_b = \begin{bmatrix} u & v & \omega \end{bmatrix}^T$ to be

$$\begin{aligned} \vec{f}_b &= m\frac{d\vec{v}_b}{dt_i} = m\left(\frac{d\vec{v}_b}{dt_b} + \vec{\omega}_b \times \vec{v}_b\right) \\ &= m\left(\begin{bmatrix} \dot{u} \\ \dot{v} \\ \dot{\omega} \end{bmatrix} + \begin{bmatrix} p \\ q \\ r \end{bmatrix} \times \begin{bmatrix} u \\ v \\ \omega \end{bmatrix}\right) \end{aligned} \tag{132}$$

i.e.

$$\begin{bmatrix} \dot{u} \\ \dot{v} \\ \dot{\omega} \end{bmatrix} = \begin{bmatrix} rv - q\omega \\ p\omega - ru \\ qu - pv \end{bmatrix} + \begin{bmatrix} f_x/m \\ f_y/m \\ f_z/m \end{bmatrix} \tag{133}$$

Let $\vec{\omega}$ and $\vec{\alpha}$ be the angular velocity vector and angular acceleration vector, respectively. Since the Newton's second law only holds in inertial frame, using the Newton's second law yields the rotational motion as

$$\vec{\tau} = J\vec{\alpha} = J\frac{d\vec{\omega}}{dt_i} \equiv \frac{d\vec{h}}{dt_i} \tag{134}$$

where J denotes the inertia of the quadrotor, $\vec{h} \equiv J\vec{\omega}$ is the angular moment and $\vec{\tau}$ denotes the external torque. Consider the quadrotor to be symmetric about three axes, the mutual inertias are $J_{xy} = J_{xz} = J_{yz} = 0$ and then the inertia is expressed by

$$J \equiv \begin{bmatrix} J_x & 0 & 0 \\ 0 & J_y & 0 \\ 0 & 0 & J_z \end{bmatrix} \tag{135}$$

Applying the Coriolis equation yields

$$\vec{\tau} = J\frac{d\vec{\omega}}{dt_i} = J\left(\frac{d\vec{\omega}}{dt_b} + \vec{\omega}_i \times \vec{\omega}\right) = \frac{d(J\vec{\omega})}{dt_b} + \vec{\omega}_i \times (J\vec{\omega}) \tag{136}$$

i.e.

$$\vec{\tau} = \frac{d\vec{h}}{dt_i} = \frac{d\vec{h}}{dt_b} + \vec{\omega}_i \times \vec{h} \tag{137}$$

Since $\vec{\tau}$ and $\vec{\omega}_i$ are applied in the body frame, we will express the Coriolis equation in the body frame with $\vec{\omega}_b = \begin{bmatrix} p & q & r \end{bmatrix}^T$, $\vec{\tau}_b = \begin{bmatrix} \tau_\varphi & \tau_\theta & \tau_\psi \end{bmatrix}^T$ and $\vec{h}_b = J\begin{bmatrix} p & q & r \end{bmatrix}^T = \begin{bmatrix} pJ_x & qJ_y & rJ_z \end{bmatrix}^T = J\vec{\omega}_b$ to be

$$\vec{\tau}_b = \frac{d\vec{h}_b}{dt_i} = \frac{d\vec{h}_b}{dt_b} + \vec{\omega}_b \times \vec{h}_b = \begin{bmatrix} \dot{p}J_x \\ \dot{q}J_y \\ \dot{r}J_z \end{bmatrix} + \begin{bmatrix} p \\ q \\ r \end{bmatrix} \times \begin{bmatrix} pJ_x \\ qJ_y \\ rJ_z \end{bmatrix} \tag{138}$$

i.e.

$$\begin{bmatrix} \dot{p} \\ \dot{q} \\ \dot{r} \end{bmatrix} = \begin{bmatrix} qr\dfrac{J_y - J_z}{J_x} \\ pr\dfrac{J_z - J_x}{J_y} \\ pq\dfrac{J_x - J_y}{J_z} \end{bmatrix} + \begin{bmatrix} \dfrac{\tau_\varphi}{J_x} \\ \dfrac{\tau_\theta}{J_y} \\ \dfrac{\tau_\psi}{J_z} \end{bmatrix} \tag{139}$$

Assume the aerodynamic forces and moments to be neglected. Fig. 4 shows the top view of the quadrotor. As shown in Fig. 5, four driving motors will produce forces F_f, F_b, F_r, F_l and torques $\tau_f, \tau_b, \tau_r, \tau_l$. The total force F applied on the quadrotor is denoted as

$$F \equiv F_f + F_b + F_r + F_l \tag{140}$$

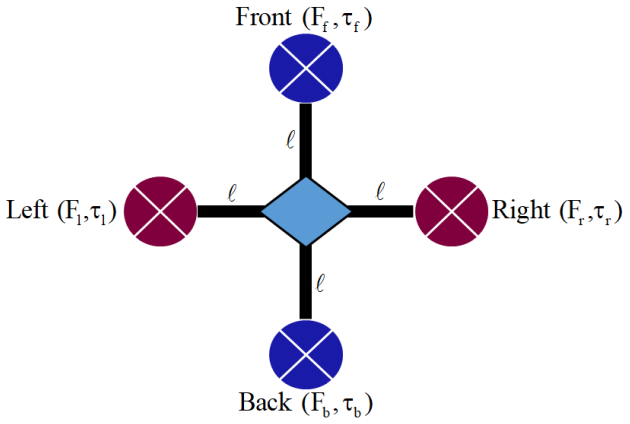

FIGURE 4. The top view of the quadrotor.

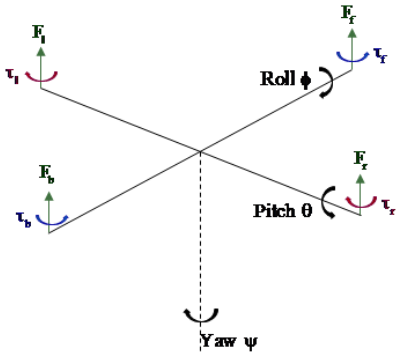

FIGURE 5. The forces and torques diagram of the quadrotor.

The gravity force acting on the quadrotor in the vehicle frame is given by

$$\vec{f}_g^{\,v} = \begin{bmatrix} 0 \\ 0 \\ mg \end{bmatrix} \tag{141}$$

Since $\vec{v}_b$ in (132) is expressed in the body frame, we will rewrite (141) in the body frame to be

$$\begin{aligned} \vec{f}_g^{\,b} \equiv \begin{bmatrix} f_x \\ f_y \\ f_z \end{bmatrix} &= \Re_v^b \vec{f}_g^{\,v} - \begin{bmatrix} 0 \\ 0 \\ F \end{bmatrix} \\ &= \begin{bmatrix} c\theta c\psi & c\theta s\psi & -s\theta \\ s\varphi s\theta c\psi - c\varphi s\psi & s\varphi s\theta s\psi + c\varphi c\psi & s\varphi c\theta \\ c\varphi s\theta c\psi + s\varphi s\psi & c\varphi s\theta s\psi - s\varphi c\psi & c\varphi c\theta \end{bmatrix} \begin{bmatrix} 0 \\ 0 \\ mg \end{bmatrix} \\ &\quad - \begin{bmatrix} 0 \\ 0 \\ F \end{bmatrix} \\ &= \begin{bmatrix} -mg\sin\theta \\ mg\sin\varphi\cos\theta \\ mg\cos\varphi\cos\theta \end{bmatrix} - \begin{bmatrix} 0 \\ 0 \\ F \end{bmatrix} \end{aligned} \tag{142}$$

Substituting (120) to (133) obtains

$$\begin{bmatrix} \dot{u} \\ \dot{v} \\ \dot{\omega} \end{bmatrix} = \begin{bmatrix} rv - q\omega \\ p\omega - ru \\ qu - pv \end{bmatrix} + \begin{bmatrix} -gs\theta \\ gs\varphi c\theta \\ gc\varphi c\theta \end{bmatrix} - \begin{bmatrix} 0 \\ 0 \\ F/m \end{bmatrix} \tag{143}$$

Assuming that φ and θ are small reduces (129) to be

$$\begin{bmatrix} \dot{\varphi} \\ \dot{\theta} \\ \dot{\psi} \end{bmatrix} = \begin{bmatrix} 1 & 0 & 0 \\ 0 & 1 & 0 \\ 0 & 0 & 1 \end{bmatrix} \begin{bmatrix} p \\ q \\ r \end{bmatrix} = \begin{bmatrix} p \\ q \\ r \end{bmatrix} \tag{144}$$

Combining (139) and (144) yields

$$\begin{bmatrix} \ddot{\varphi} \\ \ddot{\theta} \\ \ddot{\psi} \end{bmatrix} = \begin{bmatrix} \dot{p} \\ \dot{q} \\ \dot{r} \end{bmatrix} = \begin{bmatrix} qr\dfrac{J_y - J_z}{J_x} \\ pr\dfrac{J_z - J_x}{J_y} \\ pq\dfrac{J_x - J_y}{J_z} \end{bmatrix} + \begin{bmatrix} \dfrac{\tau_\varphi}{J_x} \\ \dfrac{\tau_\theta}{J_y} \\ \dfrac{\tau_\psi}{J_z} \end{bmatrix} \tag{145}$$

Differentiating (126) gives

$$\begin{bmatrix} \ddot{x} \\ \ddot{y} \\ \ddot{z} \end{bmatrix} = \begin{bmatrix} c\theta c\psi & s\varphi s\theta c\psi - c\varphi s\psi & c\varphi s\theta c\psi + s\varphi s\psi \\ c\theta s\psi & s\varphi s\theta s\psi + c\varphi c\psi & c\varphi s\theta s\psi - s\varphi c\psi \\ -s\theta & s\varphi c\theta & c\varphi c\theta \end{bmatrix} \begin{bmatrix} \dot{u} \\ \dot{v} \\ \dot{\omega} \end{bmatrix} \tag{146}$$

Neglecting the Coriolis terms p, q, r and substituting (143) into (146) give

$$\begin{bmatrix} \ddot{x} \\ \ddot{y} \\ \ddot{z} \end{bmatrix} = \begin{bmatrix} c\theta c\psi & s\varphi s\theta c\psi - c\varphi s\psi & c\varphi s\theta c\psi + s\varphi s\psi \\ c\theta s\psi & s\varphi s\theta s\psi + c\varphi c\psi & c\varphi s\theta s\psi - s\varphi c\psi \\ -s\theta & s\varphi c\theta & c\varphi c\theta \end{bmatrix} \left(\begin{bmatrix} -gs\theta \\ gs\varphi c\theta \\ gc\varphi c\theta \end{bmatrix} - \begin{bmatrix} 0 \\ 0 \\ F/m \end{bmatrix} \right) = \begin{bmatrix} 0 \\ 0 \\ g \end{bmatrix} - \begin{bmatrix} c\varphi s\theta c\psi + s\varphi s\psi \\ c\varphi s\theta s\psi - s\varphi c\psi \\ c\varphi c\theta \end{bmatrix} (F/m) \tag{147}$$

From (143) and (147), the simplified model of the quadrotor is given by

$$\ddot{\varphi} = qr\frac{J_y - J_z}{J_x} + \frac{\tau_\varphi}{J_x} \tag{148}$$

$$\ddot{\theta} = pr\frac{J_z - J_x}{J_y} + \frac{\tau_\theta}{J_y} \tag{149}$$

$$\ddot{\psi} = pq\frac{J_x - J_y}{J_z} + \frac{\tau_\psi}{J_z} \tag{150}$$

$$\ddot{x} = (-\cos\varphi \sin\theta \cos\psi - \sin\varphi \sin\psi)(F/m) \tag{151}$$

$$\ddot{y} = (-\cos\varphi \sin\theta \sin\psi + \sin\varphi \cos\psi)(F/m) \tag{152}$$

$$\ddot{z} = g - (\cos\varphi \cos\theta)(F/m) \tag{153}$$

Let the state and input variables of the quadrotor be the following quantities:
$\vec{x} \equiv [x_1\ x_2\ x_3\ x_4\ x_5\ x_6\ x_7\ x_8\ x_9\ x_{10}\ x_{11}\ x_{12}]^T, x_1 = \varphi, x_2 = \dot{\varphi}, x_3 = \theta, x_4 = \dot{\theta}, x_5 = \psi, x_6 = \dot{\psi}, x_7 = z, x_8 = \dot{z}, x_9 = x, x_{10} = \dot{x}, x_{11} = y, x_{12} = \dot{y}, u_1 = F, u_2 = \tau_\varphi, u_3 = \tau_\theta$ and $u_4 = \tau_\psi$

Therefore, the state-space mathematical model with real physical values can be represented as

$$\dot{x}_1 = x_2 \tag{154}$$

$$\dot{x}_2 = -20.52x_4x_6 + 100u_2 \tag{155}$$

$$\dot{x}_3 = x_4 \tag{156}$$

$$\dot{x}_4 = 19.07x_2x_6 + 92.59u_3 \tag{157}$$

$$\dot{x}_5 = x_6 \tag{158}$$

$$\dot{x}_6 = -0.0037x_2x_4 + 4.629u_4 \tag{159}$$

$$\dot{x}_7 = x_8 + \theta_1 \tag{160}$$

$$\dot{x}_8 = +9.8 - 0.556(\cos x_1)(\cos x_3)u_1 + \theta_2 \tag{161}$$

$$\dot{x}_9 = x_{10} \tag{162}$$

$$\dot{x}_{10} = -0.556\left[(\cos x_1)(\sin x_3)(\cos x_5) + (\sin x_1)(\sin x_5)\right]u_1 \tag{163}$$

$$\dot{x}_{11} = x_{12} \tag{164}$$

$$\dot{x}_{12} = -0.556\left[(\cos x_1)(\sin x_3)(\sin x_5) - (\sin x_1)(\cos x_5)\right]u_1 \tag{165}$$

$$y_{o1} = x_9 + x_{10} \equiv h_{o1} \tag{166}$$

$$y_{o2} = x_1 + x_2 \equiv h_{o2} \tag{167}$$

$$y_{o3} = x_3 + x_4 \equiv h_{o3} \tag{168}$$

$$y_{o4} = x_5 + x_6 \equiv h_{o4} \tag{169}$$

where $\theta_1 = \sin t, \theta_2 = \sin t$ denote to be disturbances. The initial values of the states are set to be

$$\vec{x}(0) \equiv \left[\pi/6\ \ 0\ \ \pi/6\ \ 0\ \ \pi/4\ \ 0\ \ 0\ \ 1\ \ -0.1\ \ 0.21\ \ 0.5\ \ 1\right]^T \tag{170}$$

Now we will show how to explicitly build the almost disturbance decoupling controller that tracks the desired signals $y_{od}^1 = y_{od}^2 = y_{od}^3 = y_{od}^4 = 0$ and attenuates the disturbance's effect on the output terminal. Let's arbitrarily choose $\alpha_1^1 = \alpha_1^2 = \alpha_1^3 = \alpha_1^4 = 0.02, A_c^1 = A_c^2 = A_c^3 = A_c^4 = -0.02$, $P^1 = P^2 = P^3 = P^4 = 25$ and $\nabla_{\min}^* = \nabla_{\max}^* = 25$. The optimal LQR weighting parameters Q and R are performed using PSO algorithm. Let the fitness function for LQR be the inverse of the convergence rate factor N with $N_2 = 1$ and $\Delta_{\max} = 387$. The parameter values determined for the optimization are given in Table 1. The weighting parameters Q, R and the gain K calculated for the LQR controller after optimization are given $Q = 6, R = 1$ for $\varepsilon = 0.006$ and then the solution of algebraic Riccati equation is $K = 0.803$. The fitness value for each iteration using PSO algorithm is plotted in Fig. 6.

TABLE 1. PSO optimazation parameters.

Parameter values	Definitions
$c_1 = 2; c_2 = 2$	Learning factors
$\omega = 0.6$	Inertial weighting factor
$T_{\max} = 50$	Iteration number
$Size = 10$	particle size
Velocity_max = 4	particle maximum velocity
Velocity _ min = –4	particle minimum velocity
Fun _ Ub = 0.6	particle maximum position
Fun _ Lb = 0.1	particle minimum position

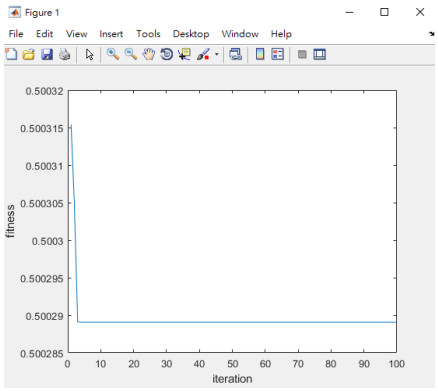

FIGURE 6. The fitness value for each iteration using PSO algorithm.

From Theorem 1, the desired almost disturbance decoupling controller is given by

$$\vec{u} = A^{-1}\left(-\vec{u}_b + \vec{u}_v + \begin{bmatrix} v_{LQR1} \\ v_{LQR2} \\ v_{LQR3} \\ v_{LQR4} \end{bmatrix}\right) \tag{171}$$

$$v_{LQR1} = -0.803\,(x_9 + x_{10}) \tag{172}$$

$$v_{LQR2} = -0.803\,(x_1 + x_2) \tag{173}$$

$$v_{LQR3} = -0.803\,(x_3 + x_4) \tag{174}$$

$$v_{LQR4} = -0.803\,(x_5 + x_6) \tag{175}$$

$$A = \begin{bmatrix} -0.45\begin{pmatrix}(\cos x_1)(\sin x_3)(\cos x_5)\\ +(\sin x_1)(\sin x_5)\end{pmatrix} & 0 & 0 & 0 \\ 0 & 100 & 0 & 0 \\ 0 & 0 & 92.6 & 0 \\ 0 & 0 & 0 & 4.63 \end{bmatrix} \tag{176}$$

$$\vec{u}_v = \begin{bmatrix} -\varepsilon^{-1}\,(0.02)\,(x_9 + x_{10}) \\ -\varepsilon^{-1}\,(0.02)\,(x_1 + x_2) \\ -\varepsilon^{-1}\,(0.02)\,(x_3 + x_4) \\ -\varepsilon^{-1}\,(0.02)\,(x_5 + x_6) \end{bmatrix} \tag{177}$$

$$\vec{u}_b = \begin{bmatrix} x_{10} \\ x_2 - 20.52x_4x_6 \\ x_4 + 19.07x_2x_6 \\ x_6 - 0.0037x_2x_4 \end{bmatrix} \tag{178}$$

$$u_1 = \frac{-1.786}{\Delta_1}\left[-x_{10} - \varepsilon^{-1}\,(0.02)\,(x_9 + x_{10}) - 0.803\,(x_9 + x_{10})\right] \tag{179}$$

$$u_2 = 0.01\left[-x_2 + 20.52x_4x_6 - \varepsilon^{-1}\,(0.02)\,(x_1 + x_2) - 0.803\,(x_1 + x_2)\right] \tag{180}$$

$$u_3 = 0.0108\left[-x_4 - 19.07x_2x_6 - \varepsilon^{-1}\,(0.02)\,(x_3 + x_4) - 0.803\,(x_3 + x_4)\right] \tag{181}$$

$$u_4 = 0.216\left[-x_6 + 0.0037x_2x_4 - \varepsilon^{-1}\,(0.02)\,(x_5 + x_6) - 0.803\,(x_5 + x_6)\right] \tag{182}$$

$$\Delta_1 \equiv (\cos x_1)(\sin x_3)(\cos x_5) + (\sin x_1)(\sin x_5) \tag{183}$$

According to the well defined assumption of the vector relative degree, it has been shown [63] that the diffeomorphism function $\phi : \Re^n \to \Re^n$ can be chosen as

$$\vec{\xi}_1 \equiv \xi_1^1 = \varphi_1^1 \equiv L_{\vec{f}}^0 h_{o1}(\vec{x}) = x_9 + x_{10}, \tag{184}$$

$$\vec{\xi}_2 \equiv \xi_1^2 = \varphi_1^2 \equiv L_{\vec{f}}^0 h_{o2}(\vec{x}) = x_1 + x_2, \tag{185}$$

$$\vec{\xi}_3 \equiv \xi_1^3 = \varphi_1^3 \equiv L_{\vec{f}}^0 h_{o3}(\vec{x}) = x_3 + x_4, \tag{186}$$

$$\vec{\xi}_4 \equiv \xi_1^4 = \varphi_1^4 \equiv L_{\vec{f}}^0 h_{o4}(\vec{x}) = x_5 + x_6, \tag{187}$$

In (184)∼(187), there are four transformed variables due to the vector relative degree of the system (154)∼(169). However, the transformed quadrotor system is not full linear and then we will design additional eight variables. Since the distributions of $\vec{g}_1(\vec{x})$, $\vec{g}_2(\vec{x})$, $\vec{g}_3(\vec{x})$, $\vec{g}_4(\vec{x})$ are involutive [64], the desired eight variables can be chosen according to the condition $L_{\vec{g}_j}\varphi_k(\vec{x}(t)) = 0$. Then we can choose the following eight transformed nonlinear variables:

$$\eta_5 \equiv \varphi_5 \equiv x_9 \tag{188}$$

$$\eta_6 \equiv \varphi_6 \equiv x_9 \tag{189}$$

$$\eta_7 \equiv \varphi_7 \equiv x_1 \tag{190}$$

$$\eta_8 \equiv \varphi_8 \equiv x_1 \tag{191}$$

$$\eta_9 \equiv \varphi_9 \equiv x_3 \tag{192}$$

$$\eta_{10} \equiv \varphi_{10} \equiv x_3 \tag{193}$$

$$\eta_{11} \equiv \varphi_{11} \equiv x_5 \tag{194}$$

$$\eta_{12} \equiv \varphi_{12} \equiv x_5 \tag{195}$$

The designed continuous diffeomorphism function transforms the original nonlinear quadrotor system into an equivalent controllable system, including the transformed nonlinear subsystem and the transformed linear subsystem. These variables $\xi_1^1, \xi_1^2, \xi_1^3, \xi_1^4$ and $\eta_5 \sim \eta_{12}$ denote the state variables of the transformed linear subsystem and nonlinear subsystem, respectively.

According to the general Lyapunov theorem, we define the composite Lyapunov function $V_{com}(\bar{e}, \eta)$ to be a weighted sum of $V_{non}(\eta)$ and $W(\bar{e})$ for the transformed nonlinear subsystem and the transformed linear subsystem, respectively:

$$\begin{aligned} &V_{com}\left(\bar{e}, \vec{\eta}\right) \\ &\equiv V_{non}(\vec{\eta}) + k(\varepsilon)W(\bar{e}) \\ &\equiv V_{non}(\vec{\eta}) + k(\varepsilon)\left(W^1\left(\overline{e^1}\right) + W^2\left(\overline{e^2}\right) + W^3\left(\overline{e^3}\right)\right) \end{aligned} \tag{196}$$

where $W\left(\overline{e^i}\right)$ satisfies

$$W^i\left(\overline{e^i}\right) \equiv \frac{1}{2}\overline{e^i}^T P^i \overline{e^i} \tag{197}$$

$$V_{non}(\vec{\eta}) \equiv \eta_5^2 + \cdots + \eta_{12}^2,\ \omega_{non1} \left\|\vec{\eta}\right\|^2 \leq V_{non}(\vec{\eta}) \leq \omega_{non2} \left\|\vec{\eta}\right\|^2, \quad \omega_{non1} = 1,\ \omega_{non2} = 1 \tag{198}$$

$$\vec{\rho}_{non}(t, \vec{\eta}, \bar{e}) = \left[\overline{e_1^1} - \eta_5\ \overline{e_1^1} - \eta_6\ \overline{e_1^2} - \eta_7\ \overline{e_1^2} - \eta_8\ \overline{e_1^3} - \eta_9\ \overline{e_1^3} - \eta_{10}\ \overline{e_1^4} - \eta_{11}\ \overline{e_1^4} - \eta_{12}\right]^T \tag{199}$$

$$\left\|\vec{\rho}_{non}(t, \vec{\eta}, \bar{e}) - \vec{\rho}_{non}(t, \vec{\eta}, 0)\right\|^2 = 2\left[\left(e_1^1\right)^2 + \left(e_1^2\right)^2 + \left(e_1^3\right)^2 + \left(e_1^4\right)^2\right] \leq M_{non}\left(\|\bar{e}\|\right), M_{non} = \sqrt{2} \tag{200}$$

$$\left\|\nabla_{\vec{\eta}} V_{non}\right\| = \left\|\left[2\eta_5\ 2\eta_6\ \cdots\ 2\eta_{12}\right]\right\| = 2\sqrt{\eta_5^2 + \eta_6^2 + \cdots + \eta_{12}^2} \leq \omega_{non3} \left\|\vec{\eta}\right\|, \quad \omega_{non3} = 2 \tag{201}$$

$$\nabla_t V_{non} + (\nabla_{\vec{\eta}} V)^T \vec{\rho}_{non}(t, \vec{\eta}, 0) = -2\left(\eta_5^2 + \eta_6^2 + \cdots + \eta_{12}^2\right) \leq -8\alpha_x\left(\vec{\eta}\right), \quad \alpha_x = 1 \tag{202}$$

Note that the function $V_{non}(\vec{\eta}) \equiv \eta_5^2 + \cdots + \eta_{12}^2$ in (200)(201) and (202) is a well-known Lyapunov function for transformed nonlinear subsystem [66]. The function $W^i\left(\overline{e^i}\right) \equiv \frac{1}{2}\overline{e^i}^T P^i \overline{e^i}$ in (197) is the Lyapunov function for transformed linear subsystem and then combine the Lyapunov functions V_{non} and W to build the composite Lyapunov function for overall transformed system. It can be proved that the related conditions of Theorem 1 hold if $\varepsilon = 0.006$, $k = 400\sqrt{\varepsilon}$, $r_1 = r_2 = r_3 = r_4 = 1$, $\alpha_s = 1.00058$, $H_{11} = 2$, $N = 1.99884$, $\vec{B}_{r_1} = \vec{B}_{r_2} = \vec{B}_{r_3} = \vec{B}_{r_4} = 1$, $K_{11} = K_{21} = K_{31} = K_{41} = -0.803$, $N_2 = 1$, $H_{22} = \frac{1}{25\varepsilon} - 8\left(\sqrt{\frac{0.0004}{\varepsilon^2} + \frac{Q}{R}} - \frac{0.02}{\varepsilon}\right)$, $H_{12} = \frac{-0.02}{\varepsilon^{\frac{1}{4}}}$. Hence the almost disturbance decoupling controllers will drive the tracking errors of the closed-loop system to zero by Theorem 1. The tracking errors of the quadrotor system with LQR (epsion=0.006) using PSO are depicted in Fig. 7. Applying the feedback linearization controller with the optimal control LQR using PSO can indeed make the tracking errors be zero and satisfy the conditions of almost disturbance decoupling performance. From Fig. 8 ∼ Fig. 11, a significant conclusion can be drawn that the control input amplitude with LQR is smaller than that without LQR. From (47) and (49), Fig. 12∼ Fig. 15 show that the convergent rates with smaller epsion value is better than a larger epsion value. Observing Fig. 16 and Fig. 19 shows that the convergence rate with optimal controller using PSO algorithm is larger than the conventional trial and error method with non-optimal controller.

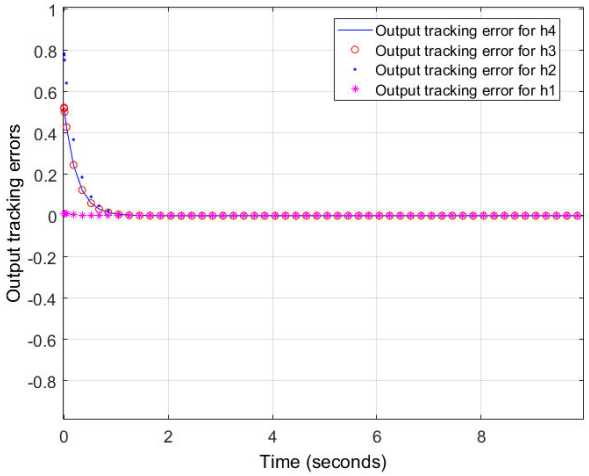

FIGURE 7. The output tracking errors using PSO (epsion=0.006).

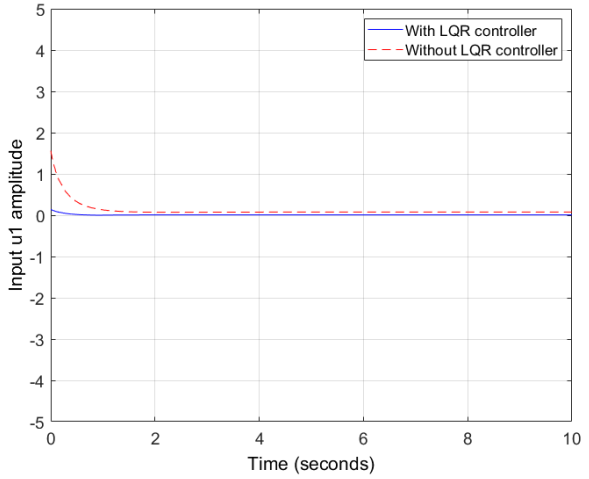

FIGURE 8. The designed controller u1 with/without LQR controller (epsion=0.006).

V. COMPARATIVE EXAMPLES TO EXISTING APPROACHES

In order to show the superiority of the proposed controller, this section will compare the performances with other existing techniques, such as famous fuzzy controller [68], and the singular perturbation method with high-gain feedback [51] shown as follows.

The block diagram of the fuzzy control is shown in Fig. 20. In general, the tracking error $e(t)$ and its time derivative $\dot{e}(t)$ are utilized as the input fuzzy variables of the IF-THEN control rules and the output is the control variable u_{fuzzy}. To make it easier to compute, the membership functions of the linguistic terms for $e(t)$, $\dot{e}(t)$ and u_{fuzzy} are all chosen to be the triangular shape functions. We define seven linguistic terms: PB(Positive big), PM(Positive medium), PS(Positive small), ZE(Zero), NS(Negative small), NM(Negative medium) and NB(Negative big), for each fuzzy variable as shown in Fig. 21∼ Fig. 23. Fuzzy control rule table for u_{fuzzy} is shown in Table 2. The rule base is heuristically built by the standard Macvicar-Whelan rule base for usual servo control systems. The Mamdani method is used for fuzzy inference.

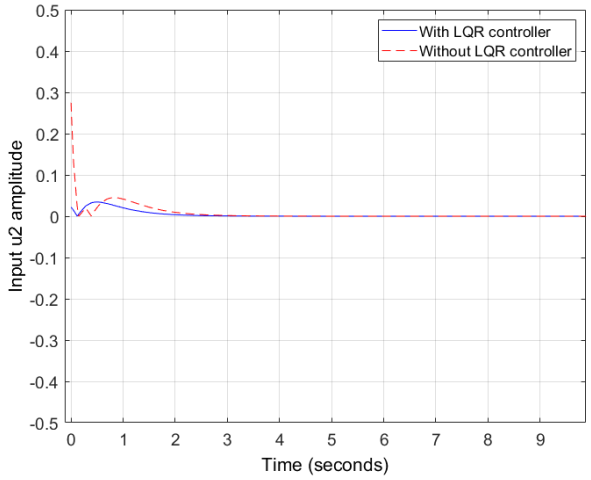

FIGURE 9. The designed controller u2 with/without LQR controller (epsion=0.006).

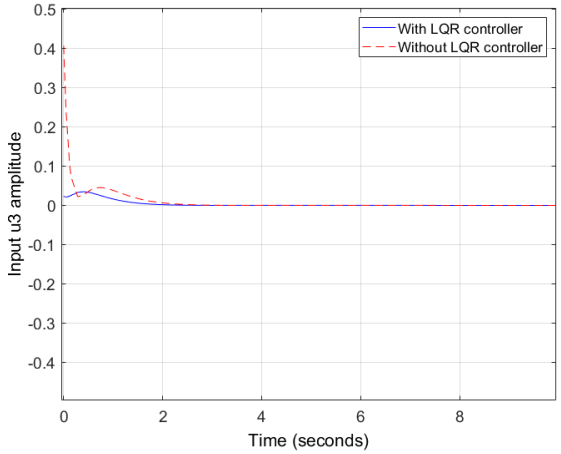

FIGURE 10. The designed controller u3 with/without LQR controller (epsion=0.006).

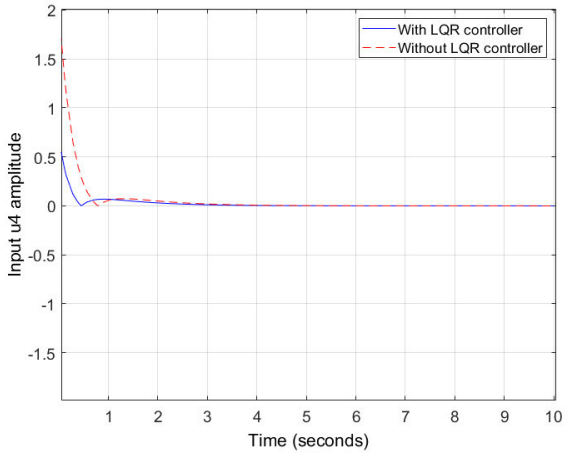

FIGURE 11. The designed controller u4 with/without LQR controller (epsion=0.006).

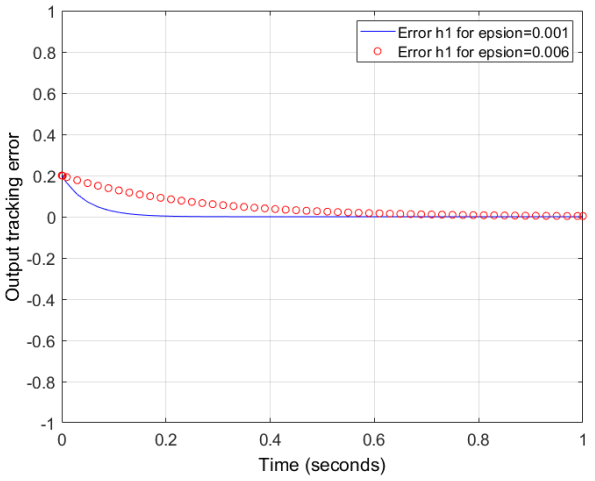

FIGURE 12. The output tracking error for h1 with larger/smaller epsion.

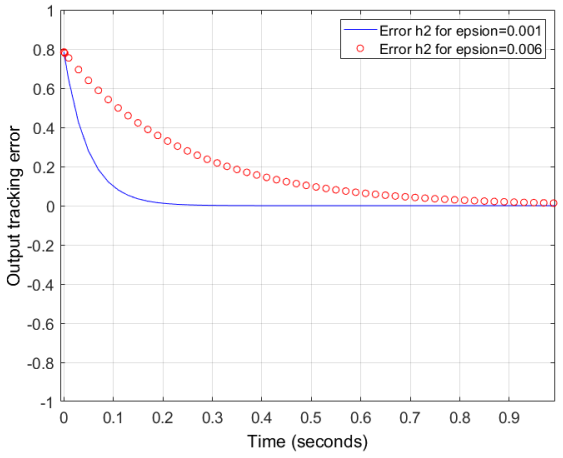

FIGURE 13. The output tracking error for h2 with larger/smaller epsion.

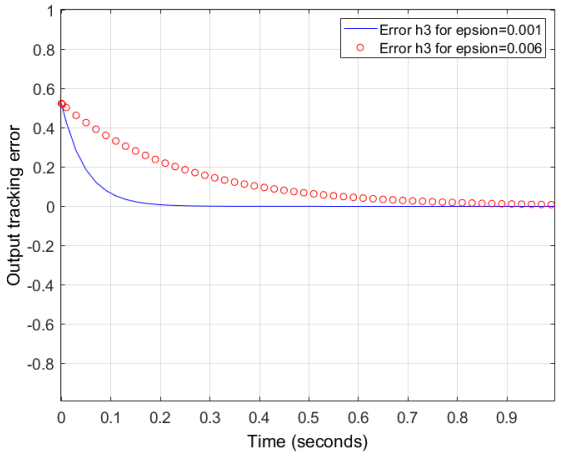

FIGURE 14. The output tracking error for h3 with larger/smaller epsion.

The defuzzification of the output set membership value is obtained by the centroid method.

In what follows, simulations of the fuzzy controller for the quadrotor system are shown. Tracking error responses for outputs h1 to h4 with the help of fuzzy toolbox for matlab, respectively are given in Fig. 24∼ Fig. 27.

Observing Fig. 24∼ Fig. 27 shows that the convergence rate with our proposed optimal controller using the PSO algorithm is larger than the conventional fuzzy controller.

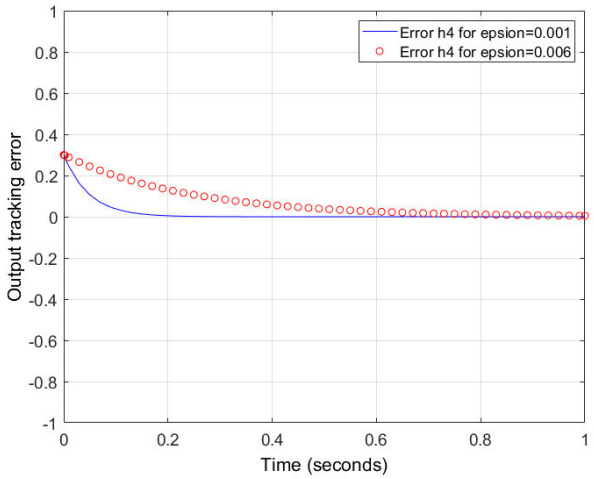

FIGURE 15. The output tracking error for h4 with larger/smaller epsion.

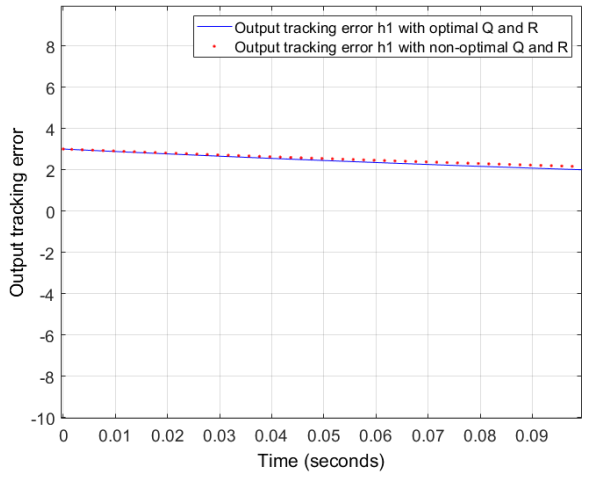

FIGURE 16. The output tracking errors with optimal/non-optimal Q and R using PSO algorithm (epsion=0.006).

TABLE 2. Fuzzy control rule base.

u_{fuzzy}		$e(t)$						
		NB	NM	NS	ZE	PS	PM	PB
$\dot{e}(t)$	NB	PB	PB	PB	PB	PM	PS	ZE
	NM	PB	PB	PB	PM	PS	ZE	NS
	NS	PB	PB	PM	PS	ZE	NS	NM
	ZE	PB	PM	PS	ZE	NS	NM	NB
	PS	PM	PS	ZE	NS	NM	NB	NB
	PM	PS	ZE	NS	NM	NB	NB	NB
	PB	ZE	NS	NM	NB	NB	NB	NB

Next, we will compare proposed approach with the singular perturbation method under high-gain feedback [50] to show that the performance of proposed design is better than it.

Reference [51] had shown that the almost disturbance decoupling performance cannot be achieved for the following

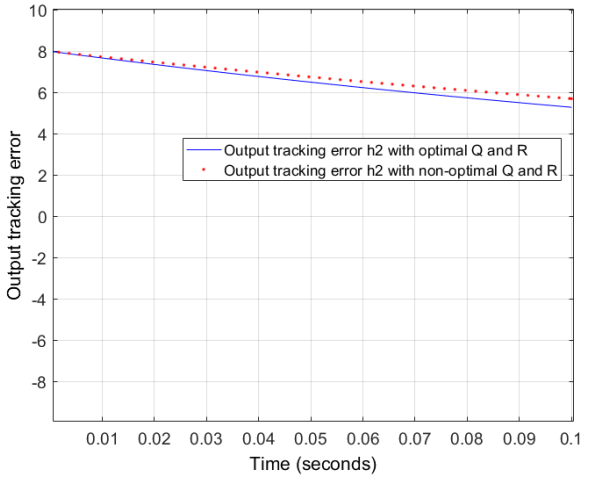

FIGURE 17. The output tracking errors with optimal/non-optimal Q and R using PSO algorithm (epsion=0.006).

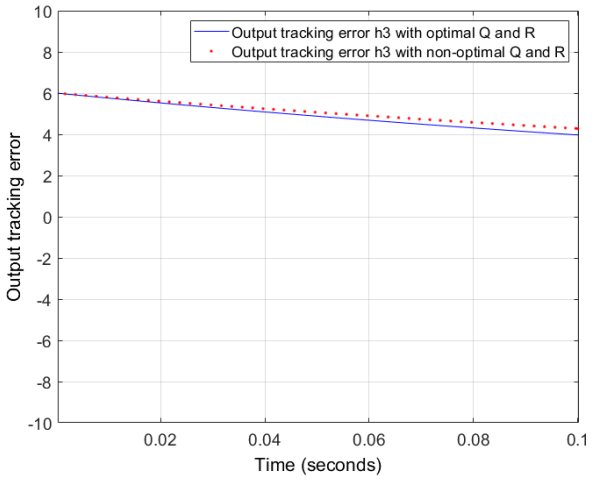

FIGURE 18. The output tracking errors with optimal/non-optimal Q and R using PSO algorithm (epsion=0.006).

nonlinear systems:

$$\begin{bmatrix} \dot{x}_1(t) \\ \dot{x}_2(t) \end{bmatrix} = \begin{bmatrix} x_2 \\ 0 \end{bmatrix} + \begin{bmatrix} 0 \\ 1 \end{bmatrix} u + \begin{bmatrix} w_1(t) \\ x_2^3 w_2(t) \end{bmatrix}, \tag{203}$$

$$y(t) = x_1(t) := h(X(t)) \tag{204}$$

where u, y_{o1} denote the input and output, respectively, $w_1(t) = w_2(t) = 0.1 \sin t$ are disturbances and the desired tracking signal is $\sin t$. The sufficient criterion in [50] requires that the nonlinearity multiplied by the disturbance satisfies the structural triangle criterion. It will be easy to calculate the following items: $L_f^0 h_{o1} = h_{o1} = x_1, dh_{o1} = [1\ 0]$, $L_f^1 h_{o1} = x_2, L_{q_2^*} L_f^1 h_{o1} = x_2^3$ and $d\left(L_{q_2^*} L_f^1 h_{o1}\right) = \left[0\ 3x_2^2\right]$. Hence the sufficient criterion of [51] is not satisfied, since $d\left(L_{q_2^*} L_f^1 h_{o1}\right) \notin span\{dh_{o1}\}$. Then the almost disturbance decoupling performance is not achieved for this system. On the contrary, this performance can be easily achieved

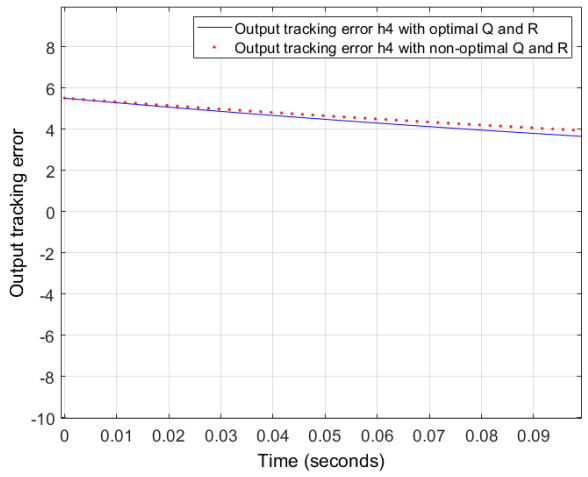

FIGURE 19. The output tracking errors with optimal/non-optimal Q and R using PSO algorithm (epsion=0.006).

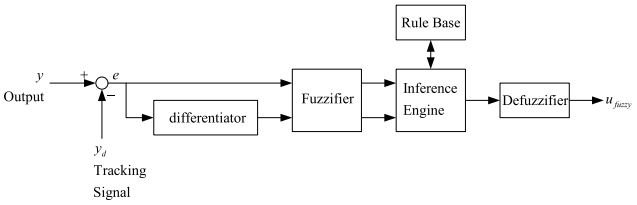

FIGURE 20. Fuzzy logic controller.

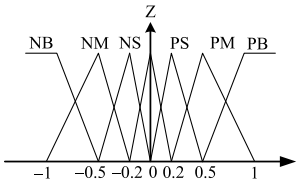

FIGURE 21. Membership functions for $e(t)$.

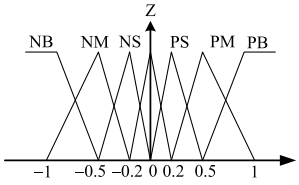

FIGURE 22. Membership functions for $\dot{e}(t)$.

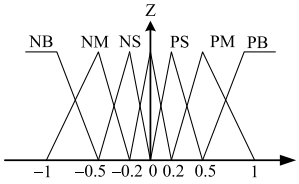

FIGURE 23. Membership functions for u_{fuzzy}.

via the proposed approach in this study. Applying the similar effective algorithm shown in Figure 2, the tracking problem with almost disturbance decoupling performance

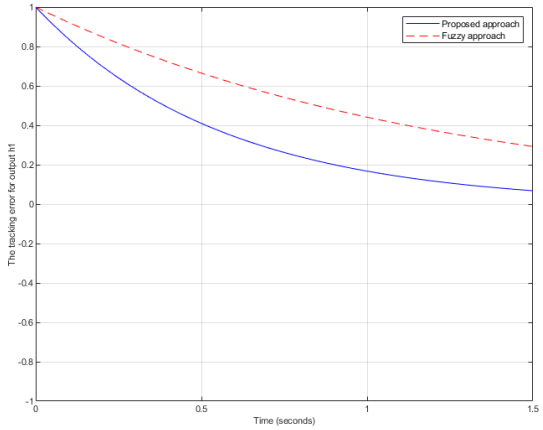

FIGURE 24. The output tracking errors for h1.

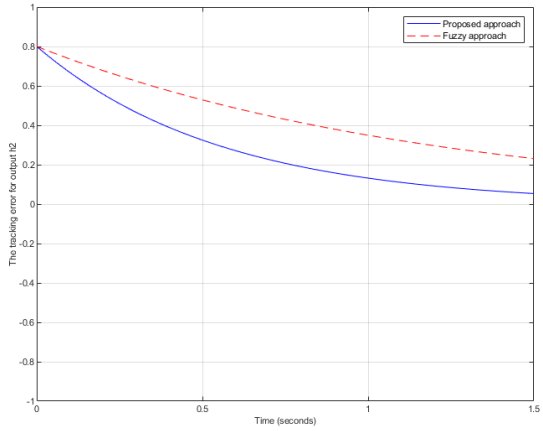

FIGURE 25. The output tracking errors for h2.

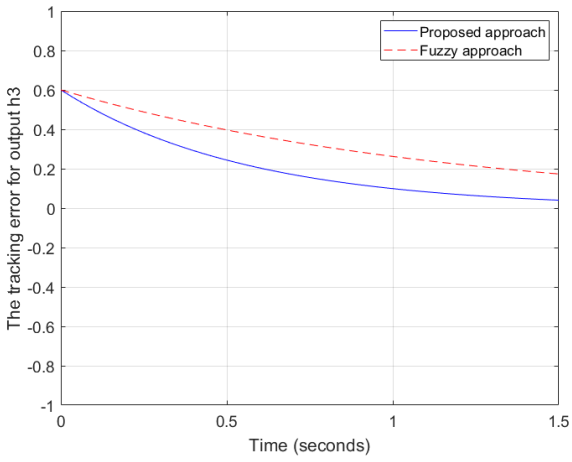

FIGURE 26. The output tracking errors for h3.

can be solvable by the state feedback stabilized controller defined by

$$u = (100/9)(x_2 - \cos t) - (10000/81)(x_1 - \sin t) - \sin t \tag{205}$$

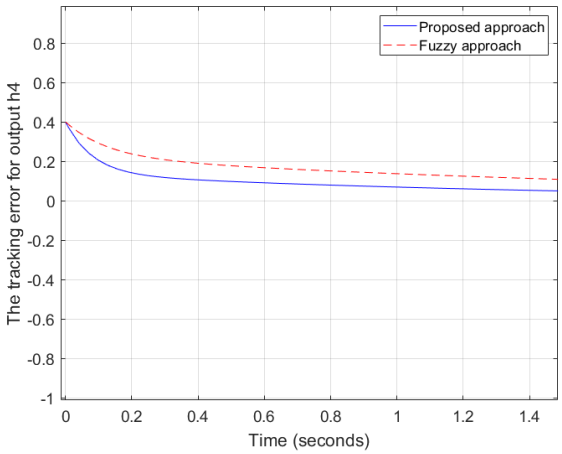

FIGURE 27. The output tracking errors for h4.

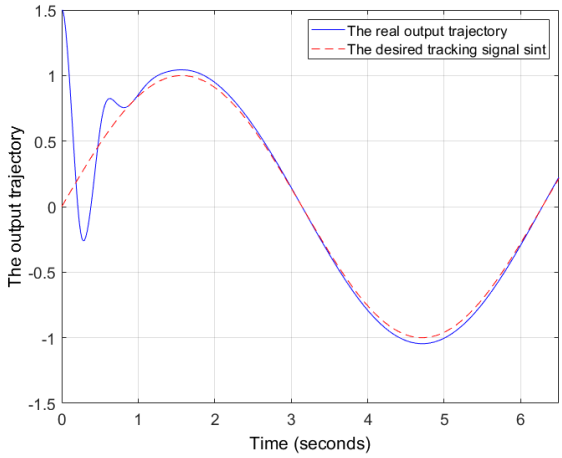

FIGURE 28. The output trajectory of feedback-controlled system for (203).

The output trajectory of feedback-controlled system for Eq. (203) is shown in Figure 28.

VI. CONCLUSION

The novel COVID-19 virus continues to spread. In this incident, agricultural spraying quadrotors are expected to develop cross-domain applications. The important mission stimulates us to design the stabilizing controller of the highly nonlinear quadrotor system by combining the feedback linearized method and LQR method using PSO. Because disturbance has a critical impact on quadrotor, this study adopts stricter almost disturbance decoupling requirement, i.e., in addition to the absolute value condition and integration condition of the tracking error, it must also meet the strict requirement of the input-to-state stable condition.

This article "firstly" proposes the convergence rate formula of the nonlinear system and uses it as the fitness function of LQR approach by using PSO to take the place of the trial and error method for traditional LQR method. Moreover, the significant innovation of the proposed method is to own "simultaneously" additional performances including the input amplitude reduction, tuning parameter optimization and globally exponential stability performances. Two comparative examples verify the fact that the convergence rate with our proposed controller is larger than the fuzzy controller, and better than the singular perturbation method with high-gain feedback. Because of the pivotal importance of quadrotor and the research results of this study, in the future, we will develop toward quadrotor with loading and formation execution tasks.

ACKNOWLEDGMENT

This work is supported by City College of Dongguan University of Technology, Grant No.: 2017YZDYB01Z, Grant Title: Create a new theory and technology of electric circuit and electronics science based on Chen's Electrical Unifying Approach.

REFERENCES

[1] D. Kapoor, D. Deb, A. Sahai, and H. Bangar, "Adaptive failure compensation for coaxial rotor helicopter under propeller failure," in *Proc. Amer. Control Conf. (ACC)*, Montreal, QC, Canada, Jun. 2012, pp. 2539–2544.

[2] J. Liu, J. Zhang, and F. Zhao, "Feature for distinguishing propeller-driven airplanes from turbine-driven airplanes," *IEEE Trans. Aerosp. Electron. Syst.*, vol. 46, no. 1, pp. 222–229, Jan. 2010.

[3] "Longitudinal stability analysis of business jet aircraft," in *Proc. Int. Conf. Eng. Emerg. Technol. (ICEET)*, Lahore, Pakistan, Feb. 2019, pp. 1–7.

[4] Y. Liu, D. Deb, and G. Tao, "Modeling and multivariable adaptive control of aircraft with synthetic jet actuators," in *Proc. 7th World Congr. Intell. Control Autom.*, Chongqing, China, 2008, pp. 2192–2199.

[5] N. Konishi, H. Fujimoto, Y. Watanabe, K. Suzuki, H. Kobayashi, and A. Nishizawa, "Lift control of electric airplanes by using propeller slipstream for safe landing," in *Proc. IEEE Int. Conf. Mechatronics (ICM)*, Nagoya, Japan, Mar. 2015, pp. 335–340.

[6] K. Takahashi, H. Fujimoto, Y. Hori, H. Kobayashi, and A. Nishizawa, "Modeling of propeller electric airplane and thrust control using advantage of electric motor," in *Proc. IEEE 13th Int. Workshop Adv. Motion Control (AMC)*, Yokohama, Japan, Mar. 2014, pp. 482–487.

[7] J. McBride, "Flight control system for small high-performance UAVs," Ph.D. dissertation, School Eng., Virginia Commonwealth Univ., Richmond, VA, USA, 2010.

[8] H. Bouadi, "Contribution to flight control law design and aircraft trajectory tracking," Ph.D. dissertation, Dept. Autom., INSA Toulouse, Toulouse, France, 2013.

[9] D. Falanga, K. Kleber, S. Mintchev, D. Floreano, and D. Scaramuzza, "The foldable drone: A morphing quadrotor that can squeeze and fly," *IEEE Robot. Autom. Lett.*, vol. 4, no. 2, pp. 209–216, Apr. 2019.

[10] M. K. M. Jaffar, M. Velmurugan, and R. Mohan, "A novel guidance algorithm and comparison of nonlinear control strategies applied to an indoor quadrotor," in *Proc. 5th Indian Control Conf. (ICC)*, New Delhi, India, Jan. 2019, pp. 466–471.

[11] S. N. Tiwari and R. Padhi, "Simultaneous attitude control and trajectory tracking of a micro quadrotor: A SNAC aided nonlinear dynamic inversion approach," in *Proc. Amer. Control Conf.*, Washington, DC, USA, Jun. 2013, pp. 194–199.

[12] M. Hossny, A. El-Badawy, and R. Hassan, "Fuzzy model predictive control of a quadrotor unmanned aerial vehicle," in *Proc. Int. Conf. Unmanned Aircr. Syst. (ICUAS)*, Athens, Greece, Sep. 2020, pp. 1–4.

[13] K. Mueller, M. Fennel, and G. F. Trommer, "Model predictive control for vision-based quadrotor guidance," in *Proc. IEEE/ION Position, Location Navigat. Symp. (PLANS)*, Portland, OR, USA, Apr. 2020, pp. 50–61.

[14] D. J. Almakhles, "Robust backstepping sliding mode control for a quadrotor trajectory tracking application," *IEEE Access*, vol. 8, pp. 5515–5525, 2020.

[15] Y. Liu, B. Jiang, J. Lu, J. Cao, and G. Lu, "Event-triggered sliding mode control for attitude stabilization of a rigid spacecraft," *IEEE Trans. Syst., Man, Cybern. Syst.*, vol. 50, no. 9, pp. 3290–3299, Sep. 2020.

[16] V. K. Tripathi, A. K. Kamath, L. Behera, N. K. Verma, and S. Nahavandi, "Finite-time super twisting sliding mode controller based on higher-order sliding mode observer for real-time trajectory tracking of a quadrotor," *IET Control Theory Appl.*, vol. 14, no. 16, pp. 2359–2371, 2020.

[17] M. S. Mahmoud and M. Maaruf, "Robust adaptive multilevel control of a quadrotor," *IEEE Access*, vol. 8, pp. 167684–167692, 2020.

[18] W. Yang, G. Cui, J. Yu, C. Tao, and Z. Li, "Finite-time adaptive fuzzy quantized control for a quadrotor UAV," *IEEE Access*, vol. 8, pp. 179363–179372, 2020.

[19] K. Alexis, G. Nikolakopoulos, and A. Tzes, "Model predictive quadrotor control: Attitude, altitude and position experimental studies," *IET Control Theory Appl.*, vol. 6, no. 12, pp. 1812–1827, 2012.

[20] J. Yang and W. X. Zheng, "Offset-free nonlinear MPC for mismatched disturbance attenuation with application to a static var compensator," *IEEE Trans. Circuits Syst. II, Exp. Briefs*, vol. 61, no. 1, pp. 49–53, Jan. 2014.

[21] B. Musmade and B. Patre, "Sliding mode control design for robust regulation of time-delay processes," *Trans. Inst. Meas. Control*, vol. 37, no. 6, pp. 699–707, Jul. 2015.

[22] J. Wang, L. Zhao, and L. Yu, "Adaptive terminal sliding mode control for magnetic levitation systems with enhanced disturbance compensation," *IEEE Trans. Ind. Electron.*, vol. 68, no. 1, pp. 756–766, Jan. 2021.

[23] M. Chen and J. Yu, "Disturbance observer-based adaptive sliding mode control for near-space vehicles," *Nonlinear Dyn.*, vol. 82, no. 4, pp. 1671–1682, Dec. 2015.

[24] Z. Dydek, A. Annaswamy, and E. Lavretsky, "Combined/composite adaptive control of a quadrotor UAV in the presence of actuator uncertainty," in *Proc. AIAA Guid., Navigat., Control Conf.*, Toronto, ON, Canada, Aug. 2010, pp. 2010–7575.

[25] G. Rigatos, P. Siano, S. Ademi, and P. Wira, "An adaptive neurofuzzy H-infinity control method for bioreactors and biofuels production," in *Proc. 43rd Annu. Conf. IEEE Ind. Electron. Soc. (IECON)*, Oct. 2017, pp. 8750–8755.

[26] J. Yang and Z. Ding, "Global output regulation for a class of lower triangular nonlinear systems: A feedback domination approach," *Automatica*, vol. 76, pp. 65–69, Feb. 2017.

[27] J. Wu, H. Zhou, Z. Liu, and M. Gu, "Ride comfort optimization via speed planning and preview semi-active suspension control for autonomous vehicles on uneven roads," *IEEE Trans. Veh. Technol.*, vol. 69, no. 8, pp. 8343–8355, Aug. 2020.

[28] L. Ming, L. Yibin, R. Xuewen, Z. Shuaishuai, and Y. Yanfang, "Semi-active suspension control based on deep reinforcement learning," *IEEE Access*, vol. 8, pp. 9978–9986, 2020.

[29] H. Chen, P.-Y. Sun, and K.-H. Guo, "A multi-objective control design for active suspensions with hard constraints," in *Proc. Amer. Control Conf.*, Jun. 2003, pp. 4371–4376.

[30] J.-S. Lin and C.-J. Huang, "Nonlinear backstepping active suspension design applied to a half-car model," *Vehicle Syst. Dyn.*, vol. 42, no. 6, pp. 373–393, Dec. 2004.

[31] C. Gohrle, A. Schindler, A. Wagner, and O. Sawodny, "Design and vehicle implementation of preview active suspension controllers," *IEEE Trans. Control Syst. Technol.*, vol. 22, no. 3, pp. 1135–1142, May 2014.

[32] L. Tang, D. Ma, and J. Zhao, "Adaptive neural control for switched non-linear systems with multiple tracking error constraints," *IET Signal Process.*, vol. 13, no. 3, pp. 330–337, 2019.

[33] L. Liu, Y. L. Liu, D. Li, S. Tong, and Z. Wang, "Barrier Lyapunov function-based adaptive fuzzy FTC for switched systems and its applications to resistance–inductance–capacitance circuit system," *IEEE Trans. Cybern.*, vol. 50, no. 8, pp. 3491–3502, Aug. 2020.

[34] R. Cui, C. Yang, Y. Li, and S. Sharma, "Adaptive neural network control of AUVs with control input nonlinearities using reinforcement learning," *IEEE Trans. Syst., Man, Cybern. Syst.*, vol. 47, no. 6, pp. 1019–1029, Jun. 2017.

[35] H. Li, Y. H. Feng, and L. Su, "Vehicle active suspension vibration control based on robust neural network," *Chin. J. Construct. Mach.*, vol. 15, no. 4, pp. 324–337, 2017.

[36] D. Y. Wang and H. Wang, "Control method of vehicle semi active suspensions based on variable universe fuzzy control," *China Mech. Eng.*, vol. 28, no. 3, pp. 366–372, 2017.

[37] S. Krim, S. Gdaim, A. Mtibaa, and M. F. Mimouni, "FPGA-based real-time implementation of a direct torque control with second-order sliding mode control and input–output feedback linearisation for an induction motor drive," *IET Electr. Power Appl.*, vol. 14, no. 3, pp. 480–491, 2020.

[38] H. Li, Z. Wang, Z. Xu, X. Wang, and Y. Hu, "Feedback linearization based direct torque control for IPMSMs," *IEEE Trans. Power Electron.*, vol. 36, no. 3, pp. 3135–3148, Mar. 2021.

[39] G. Sari, O. Akhrif, and L. Saydy, "Robust passivity-based surge control of compressors via feedback linearization," in *Proc. 9th Asian Control Conf. (ASCC)*, Istanbul, Turkey, Jun. 2013, pp. 1–5.

[40] M. Mehndiratta, E. Kayacan, M. Reyhanoglu, and E. Kayacan, "Robust tracking control of aerial robots via a simple learning strategy-based feedback linearization," *IEEE Access*, vol. 8, pp. 1653–1669, 2020.

[41] R. Rai, S. Shukla, and B. Singh, "Reactive power based MRAS for speed estimation of solar fed induction motor with improved feedback linearization for water pumping," *IEEE Trans. Ind. Informat.*, vol. 16, no. 7, pp. 4714–4725, Jul. 2020.

[42] S. Ruiz1, J. Pati, and J. Espinosa1, "PI and LQR controllers for frequency regulation including wind generation," *Int. J. Elect. Comput. Eng.*, vol. 8, no. 5, pp. 3711–3721, Oct. 2018.

[43] S. Howimanporn, S. Chookaew, and W. Sootkaneung, "Implementation of PSO based gain-scheduled PID and LQR for DC motor control using PLC and SCADA," in *Proc. Int. Conf. Control Robots (ICCR)*, Hong Kong, Sep. 2018, pp. 52–56.

[44] A. C. Unni, A. S. Junghare, V. Mohan, and W. Ongsakul, "PID, fuzzy and LQR controllers for magnetic levitation system," in *Proc. Int. Conf. Cogeneration, Small Power Plants District Energy (ICUE)*, Bangkok City, Thailand, Sep. 2016, pp. 1–5.

[45] N. A. Selamat, F. S. Daud, H. I. Jaafar, and N. H. Shamsudin, "Comparison of LQR and PID controller tuning using PSO for coupled tank system," in *Proc. IEEE 11th Int. Colloq. Signal Process. Its Appl. (CSPA)*, Kuala Lumpur, Malaysia, Mar. 2015, pp. 46–51.

[46] F. Alkhoori, S. B. Safwan, Y. Zweiri, M. N. Sahinkaya, and L. Seneviratne, "PID-LQR controllers for quad-rotor hovering mode," in *Proc. 4th Int. Conf. Syst. Informat. (ICSAI)*, Hangzhou, China, Nov. 2017, pp. 50–54.

[47] Y. Y. Nazaruddin and P. Astuti, "Development of intelligent controller with virtual sensing," *ITB J. Eng. Sci.*, vol. 41, no. 1, pp. 17–36, 2009.

[48] N. Jain, R. Gupta, and G. Parmar, "Intelligent controlling of an inverted pendulum using PSO-PID controller," *Int. J. Eng. Res. Technol.*, vol. 2, no. 12, pp. 3712–3716, 2013.

[49] B. Anditio, A. D. Andrini, and Y. Y. Nazaruddin, "Integrating PSO optimized LQR controller with virtual sensor for quadrotor position control," in *Proc. IEEE Conf. Control Technol. Appl. (CCTA)*, Copenhagen, Denmark, Aug. 2018, pp. 1603–1607.

[50] R. Marino, W. Respondek, and A. J. Van der Schaft, "Almost disturbance decoupling for single-input single-output nonlinear systems," *IEEE Trans. Autom. Control*, vol. 34, no. 9, pp. 1013–1017, 1989.

[51] R. Marino and P. Tomei, "Nonlinear output feedback tracking with almost disturbance decoupling," *IEEE Trans. Autom. Control*, vol. 44, no. 1, pp. 18–28, Jan. 1999.

[52] F. L. Lewis, D. L. Vrabie and V. L. Syrmos, *Optimal Control*. Hoboken, NJ, USA: Wiley, 2012.

[53] M. A. Mohamed, T. Jina, and W. Suc, "An effective stochastic framework for smart coordinated operation of wind park and energy storage unit," *Appl. Energy*, vol. 272, Aug. 2020, Art. no. 115228.

[54] X. Gong, F. Dong, M. A. Mohamed, E. M. Awwad, H. M. Abdullah, and Z. M. Ali, "Towards distributed based energy transaction in a clean smart island," *J. Cleaner Prod.*, vol. 273, Nov. 2020, Art. no. 122768.

[55] P. Patel, A. Shandilya, and D. Deb, "Optimized hybrid wind power generation with forecasting algorithms and battery life considerations," in *Proc. IEEE Power Energy Conf. Illinois (PECI)*, Champaign, IL, USA, Feb. 2017, pp. 1–6.

[56] M. A. Mohamed, T. Jina, and W. Suc, "Multi-agent energy management of smart islands using primal-dual method of multipliers," *Energy*, vol. 208, Oct. 2020, Art. no. 118306.

[57] H. S. Dhiman and D. Deb, "Wake management based life enhancement of battery energy storage system for hybrid wind farms," *Renew. Sustain. Energy Rev.*, vol. 130, Sep. 2020, Art. no. 109912.

[58] M. A. Mohamed, A. M. Eltamaly, and A. I. Alolah, "PSO-based smart grid application for sizing and optimization of hybrid renewable energy systems," *PLoS ONE*, vol. 11, no. 8, 2016, Art. no. e0159702.

[59] M. A. Mohamed and A. M. Eltamaly, Modeling and simulation of smart grid integrated with hybrid renewable energy systems," in *A PSO-Based Smart Grid Application for Optimum Sizing of Hybrid Renewable Energy Systems*. New York, NY, USA: Springer, 2018, pp. 53–60.

[60] M. F. Hamza, H. J. Yap, and I. A. Choudhury, "Genetic algorithm and particle swarm optimization based cascade interval type 2 fuzzy PD controller for rotary inverted pendulum system," *Math. Problems Eng.*, vol. 2015, Jun. 2015, Art. no. 695965, doi: 10.1155/2015/695965.
[61] M. A. Sen and M. Kalyoncu, "Optimal tuning of a LQR controller for an inverted pendulum using the bees algorithm," *J. Autom. Control Eng.*, vol. 4, no. 5, pp. 384–387, 2016.
[62] R. Eberhart and J. Kennedy, "A new optimizer using particle swarm theory," in *Proc. 6th Int. Symp. Micro Mach. Human Sci.*, vol. 1, Nagoya, Japan, Oct. 1995, pp. 39–43.
[63] A. Isidori, *Nonlinear Control System*. New York, NY, USA: Springer-Verlag, 1989.
[64] A. Isidori and C. I. Byrnes, "Output regulation of nonlinear systems," *IEEE Trans. Autom. Control*, vol. 35, no. 2, pp. 131–140, Feb. 1990.
[65] H. K. Khalil, *Nonlinear Systems*. Upper Saddle River, NJ, USA: Prentice-Hall, 1996.
[66] R. Marino and P. V. Kokotovic, "A geometric approach to nonlinear singularly perturbed control systems," *Automatica*, vol. 24, pp. 31–41, 1988.
[67] R. Beard, *Quadrotor Dynamics and Control*. Provo, UT, USA: Brigham Young Univ., 2008.
[68] H. S. Dhiman and D. Deb, "Fuzzy TOPSIS and fuzzy COPRAS based multi-criteria decision making for hybrid wind farms," *Energy*, vol. 202, Jul. 2020, Art. no. 117755.

CHUNG-CHENG CHEN was born in Taiwan. He received the bachelor's degree from National Taiwan Normal University, Taiwan, in 1982, and the master's and Ph.D. degrees in electrical engineering from National Sun Yat-Sen University, Taiwan, in 1987 and 1994, respectively. He joined the faculty of the Department of Electrical Engineering, National Formosa University, in 1989, as a Lecturer. He received the Ph.D. degree and became a Professor at National Formosa University, in 2000. Since 2008, he has joined the faculty of the Department of Electrical Engineering, National Chiayi University. He joined the faculty of the Department of Electrical Engineering, Hwa Hsia University of Technology, in 2011, as a Professor and the Dean of College of Information Technology and Engineering (02/2015∼07/2015), CEO of the General Knowledge Committee (08/2015∼07/2016) and Principal Secretary (08/2016∼07/2017), and invited as the Dean of the College of Electronic Engineering and Intelligent Manufacturing, City College of Dongguan University of Technology, China, in 2017. His research interests include biomedical engineering (HIV and cancer), neural networks, fuzzy control, nonlinear control theory and design, feedback linearization control, singularly perturbed systems and signal processing. He is currently the Head of the Chen's Electric Unifying Approach Research and Development team.

YEN-TING CHEN received the bachelor's degree in automatic control engineering from Feng Chia University, Taiwan, in June 2019. He is currently pursuing the master's degree with the Institute of Electrical Engineering, National Chung Hsing University. He has the special professional licenses including audio-visual electronic Bsingle chip practical level and Web design. He have received professional awards including the excellent Award of 2014 Asian Robot Sports Competition Vocational High School Bthe first prize of The 2014 Regional Teaching Resource Center Three Innovations Competition and the second prize of North Region Teaching Resource Center to Optimize Vocational School Competitions. He is currently an important member of the Chen's Electric Unifying Approach Research and Development team.